Tropical Tropospheric Ozone Trends (1998 to 2023): New Perspectives from SHADOZ, IAGOS and OMI/MLS Observations   *Revisions-18 July 2025*

Anne M. Thompson[1,2*], Ryan M. Stauffer[1], Debra E. Kollonige[1,3], Jerald R. Ziemke[1,4], Bryan J. Johnson[5], Gary A. Morris[5], Patrick Cullis[5], María Cazorla[6], Jorge Andres Diaz[7], Ankie Piters[8], Igor Nedeljkovic[8], Truus Warsodikromo[9], Francisco Raimundo Silva[10], E. Thomas Northam[11], Patrick Benjamin[12], Thumeka Mkololo[13], Tshidi Machinini[13], Christian Félix[14], Gonzague Romanens[14], Syprose Nyadida[15], Jérôme Brioude[16], Stéphanie Evan[16], Jean-Marc Metzger[16], Ambun Dindang[17], Yuzaimi B Mahat[17], Mohan Kumar Sammathuria[17], Norazura Binti Zakaria[17], Ninong Komala[18], Shin-Ya Ogino[19], Nguyen Thi Quyen[20], Francis S. Mani[21], Miriama Vuiyasawa[21], David Nardini[22], Matthew Martinsen[23], Darryl T. Kuniyuki[24], Katrin Müller[25], Pawel Wolff[26], Bastien Sauvage[27]

*Corresponding author: Anne M. Thompson (anne.m.thompson@nasa.gov)

[1]NASA/Goddard Space Flight Center (GSFC), Greenbelt, MD, USA anne.m.thompson@nasa.gov; ORCID: 0000-0002-7829-0920; ryan.m.stauffer@nasa.gov; ORCID: 0000-0002-8583-7795; [2]University of Maryland-Baltimore County, Baltimore, MD 21228; [3]Science Systems and Applications, Inc., Lanham, MD, debra.e.kollonige@nasa.gov; ORCID: 0000-0002-6597-328X; [4]Morgan State Univ., Baltimore, MD, jerald.r.ziemke@nasa.gov; ORCID: 0000-0002-5575-3654; [5]NOAA/Global Monitoring Lab, Boulder, CO; [6]Universidad San Francisco de Quito USFQ, Colegio de Ciencias e Ingenierías, Instituto de Investigaciones Atmosféricas, Quito, Ecuador; mcazorla@usfq.edu.ec; https://orcid.org/0000-0001-5295-2968; 7 - Universidad de Costa Rica, San Jose, Costa Rica, jorge.andres.diaz@gmail.com; 8 - Royal Netherlands Meteorological Institude (KNMI), De Bilt, The Netherlands, ankie.piters@knmi.nl, igor.nedeljkovic@knmi.nl; 9 - Meteorological Service of Surinam, Paramaribo, Surinam, wtruus98@gmail.com; 10 - Brazilian National Institute of Space Research (INPE), Natal, Brazil, fraimundo@crn.inpe.br; 11 – Science Systems and Applications, Inc., Wallops Island, VA., USA, e.thomas.northam@nasa.gov; 12 – US Space Force Base, Patrick, FSB, FL, USA, Yang Enterprises, Inc., patrick.benjamin.1.ctr.gb@spaceforce.mil; 13 - South African Weather Service (SAWS), Pretoria, South Africa, thumeka.mkololo@weathersa.co.za, tshidi.machinini@weathersa.co.za; 14 – MeteoSwiss, Payerne, Switzerland, christian.felix@meteoswiss.ch, gonzague.romanens@meteoswiss.ch; 15 - Kenya Meteorological Department, Nairobi, Kenya, syprosenyadida1@gmail.com; 16 - Université de La Réunion, Laboratoire de l'Atmosphère et des Cyclones (LACy), La Réunion, France, jerome.brioude@univ-reunion.fr, stephanie.evan@univ-reunion.fr, jean-marc.metzger@univ-reunion.fr; 17 - Malaysian Meteorological Department, Petaling Jaya, Malaysia, ambun@met.gov.my, yuzaimi@met.gov.my, mohan@met.gov.my, norazura@met.gov.my; 18 - National Research and Innovation Agency (BRIN), Bandung, Indonesia, ninongk@yahoo.com;ORCID: 0000-0003-3869-9622; 19 - Japan Agency for Marine-Earth Science and Technology (JAMSTEC), Research Institute for Global Change, Yokosuka, Japan, ogino-sy@jamstec.go.jp; 20 - Aero-Meteorological Observatory (AMO), Viet Nam Meteorological and Hydrological Administration, quyenck@gmail.com; 21 - The University of the South Pacific (USP), Suva, Fiji, francis.mani@usp.ac.fj, miriamavuiyasawa@gmail.com; 22 - david.nardini@noaa.gov; 23- CIRES, Univ. Colorado, Boulder, CO, matthew.martinsen@noaa.gov; 24 – NOAA/GML, Boulder, CO; darrylt.kuniyuki@noaa.gov 25 - Alfred - Wegener – Institut, Helmholtz Centre for Polar and Marine Research, Potsdam, Germany, katrin.mueller@awi.de; 26- SEDOO, Univ. Paul Sabatier III, Toulouse, France; now at ECMWF, Bonn, Germany, pawel.wolff@ecmwf.int; ORCID: 0000-0002-2082-6825; 27- Laboratoire d'Aérologie Observatoire Midi-Pyrénées, 14 av. E. Belin, 31400 Toulouse France; Bastien.sauvage@univ-tlse3.fr; ORCID : 0000-0003-3410-2139

Keywords: **Ozonesondes, Ozone Trends, Lower Stratosphere, Satellite Ozone, SHADOZ, IAGOS**

Abstract. Tropospheric ozone trends are important indicators of climate forcing and surface pollution yet relevant satellite observations are too uncertain for assessments. The assessment project TOAR-II has used multi-instrument, ground-based data for global trends over 2000-2022 (Van Malderen et al., 2025a,b). For the tropics trends are derived from SHADOZ ozonesonde profiles (Thompson et al., 2021, "T21"; Stauffer et al., 2024) or combinations of satellite, SHADOZ and IAGOS aircraft measurements (Gaudel et al., 2024). We extend T21 that covered 1998-2019, analyzing SHADOZ data at 5 sites with a Multiple Linear Regression (MLR) model for 1998-2023, and reporting trends for two free tropospheric (FT) segments, lowermost stratosphere and total tropospheric column ($TrCO_{sonde}$). Trends for the Aura period, 2005-2023, are computed from OMI/MLS $TrCO_{satellite}$. We find: (1) Extending SHADOZ analyses four years shows little change from T21; $TrCO_{sonde}$ trends are small (0.5-1 DU/dec) except over SE Asia. (2) Annual trends for $TrCO_{sonde}$ and OMI/MLS $TrCO_{satellite}$ agree within uncertainties at 4 of 5 sites. Sensitivity tests show*: (1) adding thousands of FT IAGOS profiles to SHADOZ yields little change in trends; SHADOZ sampling is sufficient. (2) QR and MLR median trends are both near-zero but QR captures extremes (5%-ile, 95-%ile) with changes up to ±1 DU/decade ($p < 0.10$). (3) Twelve-year analyses for trends lead to uncertainty changes too large for an assessment. This study and Van Malderen et al. (2025a;b) provide the most reliable TOAR-II trends to date: over the past ~25 years, tropical FT ozone changes are modest, ~(-3-+3)%/decade, except over SE Asia.

1 Introduction

The importance of tropical tropospheric ozone in atmospheric composition and climate variability

has long been known (Lacis et al., 1990; Schwartzkopf and Ramaswamy, 1993). Although the thickness

of total column ozone (TrCO) in the tropics (~250-325 Dobson Units, DU; 1 DU=$2.69 \times 10^{16} cm^{-2}$) is much

less than in the extra-tropics (350-450 DU), the latitude band from -30° to +30° covers roughly 1/2 of

the Earth's surface. In this region tropospheric ozone is a major source of global OH (hydroxyl radical),

key to Earth's oxidizing capacity (Thompson et al., 1992), controlling the lifetimes of countless biogenic

and anthropogenic species. Global OH also controls the lifetime of methane, a powerful greenhouse gas

with both natural and anthropogenic sources (Khalil, 2000). Methane (CH_4) increases alone add ozone

to the troposphere and methane's oxidation by OH to carbon monoxide (CO), that also affects the

amount of OH, establishes a feedback cycle among O_3-OH-CH_4-CO (Thompson and Cicerone, 1986;

Thompson et al., 1990). Regional variability in factors controlling the cycle derives from local levels of

the shorter-lived nitrogen oxides and reactive volatile organic compounds. The tropics/subtropics (-30°

to +30°) is where the "tropical pipe" (Plumb, 1996) carries ozone and ozone-destroying trace species

from the tropics into the mid-latitude lowermost stratosphere (LMS).

Trends in tropical tropospheric and LMS ozone are of interest for several reasons. First, free

tropospheric (FT) ozone is an important greenhouse gas. There is a potential for significant changes in

FT ozone because parts of the tropics are in areas of rapid changes in emissions. These may be caused

by economic development (Zhang et al., 2016) and/or variations in land-use and fire activity

(Christensen et al., 2022; Tsivlidou et al., 2023). Second, with relatively low ozone amounts relative to

the extra-tropics, ozone near the tropical tropopause is highly sensitive to dynamical interactions

Randel et al. (2007). Analyses of ozone profiles over the past ~25 years have found regional

meteorological changes propagating to seasonal ozone increases. Stauffer et al. (2024) verified that a suspected decline in early-year convection (Thompson et al., 2021; hereafter T21) drove 1998-2022 ozone increases over equatorial southeast Asia. New reports on decreasing tropical cloud cover (Tselioudis et al., 2025) and a shift in ITCZ location (Aumann et al., 2024) may indicate changes in convection. At Réunion Island shifting anticyclones caused an increase in FT ozone from 1998-2023 (Millet et al., 2025). Recurring influences of climate oscillations on FT and LMS ozone are well-documented in ozonesonde and satellite data (Thompson et al., 2001; Ziemke et al., 2003; Ziemke et al., 2006; Ziemke et al., 2019; Lee et al., 2010; Randel and Thompson, 2011; Thompson et al., 2011).

1.1 The TOAR Project. Challenges in Assessing Tropospheric Ozone Trends

Context for this study comes from the International Global Atmospheric Chemistry/Tropospheric Ozone Assessment Report (IGAC/TOAR) that is completing its second phase, TOAR II, initiated in 2020. The first TOAR, designated here as TOAR I and published as a collection of 11 papers in *Elementa*, 2017-2020; https://online.ucpress.edu/elementa/toar) included an assessment of surface ozone changes (Chang et al., 2017) based on a vast set of surface ozone measurements from 7 continents (Schultz et al., 2017). However, because the FT is the region of greatest radiative forcing by ozone, the trends community needs profile data. Ozone observations for the FT are relatively sparse. A TOAR I evaluation by Tarasick et al. (2019) pointed out the uneven geographic coverage of ozone profiles from soundings (~60 publicly available station records since the early 1990s) and aircraft landing and takeoff profiles to ~250 hPa that are used for FT ozone analyses. Tarasick et al. (2019) also questioned the suitability of all ground-based (sonde, aircraft, lidar, passive spectrometers) for monitoring FT ozone using illustrations from multi-decadal records that include obsolete techniques, evolving versions of instruments and/or inconsistent absolute calibration. Nonetheless, several follow-on studies to TOAR I employed sonde (T21) and commercial aircraft data (from the In-service Aircraft for a Global Observing System, IAGOS; https://iagos.org), with 5-10% accuracy or better, to estimate trends from the 1990s to ~2018 (Gaudel et al., 2020; Thouret et al., 2022).

Efforts to fill gaps with tropospheric ozone estimates from satellite data, preferred over in-situ methods for their even global coverage, have been mixed. For TOAR I Gaudel et al. (2018) pointed out that trends derived from five satellite products covering tropics and mid-latitudes for the 2005-2016 period differed from one another not only in magnitude but in sign. The newer TOAR II evaluation of six satellite products for 2015-2019 over the tropics (Gaudel et al., 2024), where satellite estimates tend to be most reliable (T21), exhibited a range of values. Not only were uncertainties among the products highly variable; comparisons of monthly mean satellite columns with sonde and IAGOS profiles up to 270 hPa exhibited r^2 correlations as low as 0.27.

123   Other TOAR II studies also reveal a persistent uncertainty in the application of satellite data for

124   trends analyses. Pope et al. (2023) published global trends from 2005-2017 OMI total column ozone

125   data that are too high because of a drift in OMI that was corrected in Gaudel et al. (2024). The latter

126   study led to a satellite-based estimate for tropical ozone trends for 2005-2019 of ~(0.5-3) ppbv/decade

127   for TrCO (tropospheric column ozone), similar or slightly larger than T21. Trends determined from non-

128   UV satellite instruments have been disappointing (Gaudel et al., 2018). A TOAR II contribution by

129   Froidevaux et al. (2025) examined changes in tropical ozone (±26 deg latitude) over the 2005 to 2020

130   period using measurements from the three lowest levels of MLS (Microwave Limb Sounder).

131   Unfortunately, the zonal structure of MLS data at the 146 hPa and 213 hPa levels (Fig. 1 in Froidevaux et

132   al., 2025) shows that the prominent ozone wave-one feature, associated with the Walker circulation

133   (Thompson et al., 2003; Thompson et al., 2017), is absent, i.e., MLS does not capture regional differences

134   as OMI-based products do. Froidevaux et al. (2025; Figs. 1, 2, 5) compare the MLS global structure to

135   ozone output at 215 and 146 hPa from 3 models, Whole Atmosphere Community Climate Model

136   (WACCM6) and two variants of the Community Atmosphere Model with Chemistry (CAM-Chem), each

137   variant using different anthropogenic emissions. The models are likewise zonally uniform in upper

138   tropospheric ozone so they do not yield meaningful tropical upper tropospheric ozone trends either.

139   A TOAR II-related investigation (Boynard et al., 2025) uses IR-based retrievals from the MetOP IASI

140   satellite instrument to determine trends for the period 2008-2023. As in Gaudel et al. (2018) the newer

141   IASI tropospheric ozone climatology differs from that of uv-based products; IASI's negative ozone trends

142   also disagree with increases from UV-based products. Boynard et al. (2025) offer little explanation for

143   the discrepancies. They note that their 12-yr period trends (2008-2019), roughly half as long as the

144   sonde or aircraft trends in T21 or Gaudel et al. (2024) may be too short for a statistically robust result.

145   Pennington et al. (2025) does provide some insight into long-term changes of 3 satellite IR products

146   (TROPESS CrIS, AIRS, AIRS+OMI) compared to ozonesondes and finds that the global tropospheric

147   ozone satellite-sonde bias is approximately one third the magnitude of trends in global tropospheric

148   ozone reported by TOAR I.

149   Keppens et al. (2025) addressed the question of whether satellite data harmonization for nadir ozone

150   profile and column products improves satellite data consistency for both their mean distributions and

151   long-term changes. They concluded that their harmonization methods reduce inter-product dispersion

152   by about 10% when comparing to global ozonesonde datasets from 43 sites, but there is a significant

153   meridional dependence, and the dispersion reduction is not consistent in space or time. This implies

154   that a substantial part of the inter-product differences is instrument and/or retrieval-specific and the

155   harmonization methods have limited application to TOAR II. An alternate method of combining the

156 residual and profile products with a column fill-in method is expected to be published as the TOAR II

157 "satellite assessment."

1.2 TOAR II Studies with Ground-based Measurements. Statistical Issues.

159 TOAR II has engaged a more globally representative set of researchers than TOAR I and reports data

160 and analyses from a larger set of observations. Dozens of TOAR II-related publications can be reviewed

161 at https://copernicus.org/articles/special_issue10_1256.html. Given the persistent uncertainty of the

162 satellite records, a number of TOAR II contributors formed a community project, the Harmonization and

163 Evaluation of Ground-based Instruments for Free-Tropospheric Ozone Measurements (HEGIFTOM), to

164 apply newly standardized ozone measurement and processing protocols for data from sondes, aircraft

165 and other ground-based (GB) instruments: FTIR, tropospheric ozone lidar and Umkehr retrievals from

166 Dobson spectrometers. The rationale is that GB networks, with stable operations at fixed sites and well-

167 calibrated instruments, e.g., as in the Network for Detection of Atmospheric Composition Change

168 (NDACC; De Mazière et al., 2018), provide suitable time-series at dozens of sites over 7 continents and

169 pole to pole. HEGIFTOM has two objectives: (1) harmonize data from ~80 long-term stations (1990s to

170 2023) in four GB networks using the most up-to-date reprocessing techniques with each record

171 referenced to absolute standards; (2) calculate trends for the 2000 to 2022 period with harmonized

172 data, reporting station trends with uncertainty. The trends for 55 individual stations are tabulated and

173 illustrated in Van Malderen et al. (2025a; referred hereafter to as HEGIFTOM-1). Regional trends based

174 on merging selected stations in densely sampled areas appear in Van Malderen et al. (2025b; referred

175 hereafter to as HEGIFTOM-2).

176 Early in the TOAR II study period we analyzed ozone profiles in the tropics collected in the Southern

177 Hemisphere Additional Ozonesondes (SHADOZ) network (Thompson et al., 2003; Thompson et al.,

178 2017) to compute FT and LMS ozone trends. The results in T21 are based on data from 8 combined

179 SHADOZ stations within ±15 degrees latitude; the Goddard Multiple-Linear Regression (MLR) model

180 calculated trends from 1998 through 2019 from the surface to 20 km. Changes in individual layers

181 between 5 and 15 km were typically (5-10)%/decade, but only seasonally; over the equatorial SE Asian

182 stations at Kuala Lumpur and Watukosek, Indonesia, some layers displayed increases up to 20%/

183 decade (Fig. 6 in T21). However, in general, annually averaged changes in equatorial regions ranged

184 from ~0 to +(1-2)%/decade or –(1-2)%/decade. In T21 LMS ozone (LMS defined as within 15-20 km)

185 computed with the MLR model displayed a seasonal loss up to 10%/decade (July through September)

186 or to 3%/decade, annually averaged. The loss maximized at ~18 km. At the same time of year, a positive

187 trend in tropopause height (TH), derived from the SHADOZ radiosondes, was detected. Redetermining

188 LMS ozone changes in the 5 km column above the tropopause zeroed out the apparent trend.

189   More recently, the Stauffer et al. (2024, referred to as S24) paper demonstrated that over the 25-

190   yr period 1998-2022, early year (February through April/May) FT ozone increases in SHADOZ data

191   are associated with declining convection, most pronounced over SE Asia but observed to a lesser

192   degree at the other stations. With the newest OMI/MLS-based satellite estimates of total

193   tropospheric column ozone (TrCO), Gaudel et al. (2024) showed that over the Aura era (2005-2019)

194   trends from satellite, SHADOZ and IAGOS aircraft profiles were in good agreement with one another

195   over southeast (SE) Asia, similar to S24. SHADOZ only (T21) and IAGOS trends (Gaudel et al., 2024)

196   diverge somewhat over the equatorial Americas and Africa, partly due to a difference in sampling

197   sites, e.g., west African IAGOS profiles in Gaudel et al. (2024) vs the SHADOZ Nairobi station.

198   **1.3 This study**

199   We use the Goddard MLR model to calculate trends in monthly mean SHADOZ data for the period

200   1998 through 2023, addressing the following questions:

201   -   Compared to T21, that reported on the 1998-2019 period, what do FT and LMS ozone

202   trends look like in the equatorial zone (-15° to +15°) with four additional years of SHADOZ

203   profiles? Because the extension covers 2020 to 2023, the comparisons are looking for impacts

204   of COVID-19 (Steinbrecht et al., 2021; Ziemke et al., 2022).

205   -   How do trends in tropospheric ozone for 1998-2023 compare to trends for 2000 to 2023?

206   In other words, is the 26-year trend biased by SHADOZ starting at the end of the 1997-1998 ENSO

207   that produced strong perturbations to tropical ozone (Thompson et al., 2001)?

208   -   How do SHADOZ total tropospheric column changes ($TrCO_{sonde}$) compare to OMI/MLS

209   column ozone trends over the 2005-2023 period? Do the satellite data capture the seasonality of

210   sonde-derived trends as noted in T21 and S24?

211   In addition to updated trends for equatorial SHADOZ sites, we have used SHADOZ profiles to

212   investigate three statistical issues raised in HEGIFTOM-1 and other TOAR II studies.

213   -   HEGIFTOM-1 calculated median trends for sondes and all other GB data using both Quantile

214   Regression (QR) and MLR models. Within the associated uncertainties of each, the two methods

215   gave identical results for annually averaged trends. Here we explore special features of QR and

216   MLR to learn more about the nature of the trends, e.g., seasonality (MLR), changes in the highest

217   and lowest quantile (QR).

218   -   Second, we use MLR to evaluate the sensitivity of trends on sample size as raised in TOAR II

219   papers (Chang et al., 2020; Chang et al., 2021; Gaudel et al. 2024) and HEGIFTOM-1 by

220   augmenting equatorial SHADOZ data with tropical IAGOS profiles for the appropriate region.

221   These calculations are carried out for FT ozone, i.e., in the region where radiative forcing is most

222   effective and both sondes and aircraft sample (700-300 hPa, roughly 5-10 km).

223   -   Satellite records are variable in length, with the most frequently used tropospheric estimates

224   starting after 2004 and a number of products merging measurements from multiple instruments.

225   We examine the sensitivity of trends to length of the observation period using QR by comparing

226   the 26-yr SHADOZ ozone trend to a recalculation that coincides with the IASI period 2008-2019

227   for which trends are reported in Boynard et al. (2025).

228   Data and analysis methods appear in **Section 2** with Results and Discussion in **Section 3. Section 4**

229   presents Summary and Conclusions.

230

231   **2. Data and Methods of Analysis**

232   **2.1 Ozone datasets**

233   Three datasets are used in our study: ozonesonde profiles from the SHADOZ network; partial ozone

234   profiles from the IAGOS commercial aircraft network; monthly-averaged OMI/MLS tropospheric ozone

235   column estimates from 2005 through 2023.

236   **2.1.1 SHADOZ ozonesonde observations**

237   **Fig. 1a** displays the SHADOZ network stations, italicized with coordinates in **Table 1.** Quito (Cazorla,

238   2016; Cazorla et al., 2021; Cazorla and Herrera, 2022) and Palau (Müller et al., 2024) soundings, taken

239   since 2014, have recently been added to the archive at https://tropo.gsfc.nasa.gov/shadoz. The ozone

240   profiles are obtained from electrochemical concentration cell ozonesondes coupled to standard

241   radiosondes as described in earlier publications, e.g., Thompson et al., 2003; Thompson et al. 2007;

242   Thompson et al., 2019. The profiles are archived with ozone uncertainties calculated with each

243   individual ozone partial pressure available as separate files at the SHADOZ archive (Witte et al., 2018;

244   WMO/GAW Rep. 268, 2021). Recent evaluations of ozonesonde data have established the quality of the

245   global ECC network. Measurements of total column ozone (TCO) from 60 global ozonesonde stations

246   average within ±2% agreement with total ozone from 4 UV-type satellites since 2005 (Stauffer et al.,

247   2022). About half the SHADOZ stations exhibit a ~3-5% dropoff in stratospheric ozone (Stauffer et al.,

248   2020) that is not completely understood (Nakano and Morofuji, 2023; Smit et al., 2024). Accordingly,

249   our study only uses ozone data below ~50 hPa, defining the lowermost stratospheric (LMS) ozone as

250   bounded by 15-20 km.

251   For the update to T21, that was based on 1998-2019 SHADOZ V06 ozonesonde data

252   (https://doi.org/10.57721/SHADOZ-V06), the same records for 8 equatorial sites, located between 5.8N

253   and 14S (color-coded in **Fig. 1b;** italicized in **Table 1**) are used with four additional years (2020-2023)

254   of ozone and P-T-U (pressure-temperature-humidity) profiles. These 8 stations have at least 14 years of

255   data between 1998 and 2023, although several have multi-year gaps (**Figs. 2, 3 Fig. S1**). For more

256   reliable statistics three of the "stations" or "sites" as they are referred to (**Fig. 1b**), are defined by

257   combining profiles from pairs of launch locations abbreviated as follows: SC-Para for San Cristóbal-

258 Paramaribo (dark blue dots in **Fig. 1b)**; Nat-Asc for Natal-Ascension (red dots in **Fig. 1b)**; KL-Java (cyan

259 dots in **Fig. 1b)** for Kuala Lumpur-Watukosek (**Table 2**). T21 (see Supplementary Material) describes

260 multiple tests that were conducted to verify that these combinations are statistically justified. Annual

261 cycles in absolute column amounts (**Fig. 2**) and anomalies for the pairs were well-correlated. In T21

262 (Supplementary Material) total tropospheric columns integrated from sondes ($TrCO_{sonde}$) at the 8

263 individual stations were also well-correlated ($r^2=0.72$) with colocated $TrCO_{satellite}$ from OMI/MLS data

264 over the period 2005-2019. It is important to note that the 8 well-correlated sites are within 15 degrees

265 latitude of the equator. The correlation falls to $r^2=0.50$ when comparisons are made between sondes and

266 satellite columns for the 4 subtropical SHADOZ stations. FT ozone at those locations are seasonally-

267 dependent mixtures of tropical and extra-tropical air masses, with latitudes (**Table 4)** spanning Hanoi

268 (+21.0) to Irene (-25.9).

269   We have also analyzed trends of tropospheric ozone column and free tropospheric ozone at

270 individual SHADOZ stations using a QR model, following column definitions and guidelines for the TOAR

271 II/HEGIFTOM project analysis (Chang et al., 2023). The tropospheric ozone column in HEGIFTOM trends

272 analysis is defined as surface to 300 hPa; the FT is defined as a layer between 300 and 700 hPa and the

273 results are given as ppbv O_3/decade change and %/decade. The QR trends for 13 SHADOZ sites from

274 2000 to 2022 are summarized in **Table 4;** a subset of them appear in an evaluation of ground-based

275 global ozone trends in HEGIFTOM-1.

276   **2.1.2 SHADOZ and IAGOS-SHADOZ blended profiles. LMS and FT ozone**

277   The MLR trend analyses (results in **Table 2 and 3**) use SHADOZ profile measurements in several

278 ways. First, the trends are computed using monthly-averaged ozone mixing ratios at 100-m intervals

279 from the surface to 20 km, as described in T21. Second, most results are illustrated as ozone column

280 amounts (in DU) for two FT segments, 5-10 km and 10-15 km, and for the LMS. Trends for ozone and P-

281 T-U data below 5 km are determined for completeness but are not tabulated because station sampling

282 times and local pollution can vary, giving artifact biases among the individual sites (Thompson et al.,

283 2014). We use 15-20 km for the LMS for two reasons. This is where several studies identified wave

284 activity associated with convection and ENSO-La Niña oscillations (Lee at al., 2010; Thompson et al.,

285 2011; Randel and Thompson, 2011; T21). Second, Randel et al. (2007) identified a distinct ozone annual

286 cycle in the 15-20 km range driven by the Brewer-Dobson circulation.

287   A third way of using SHADOZ profiles in the MLR analysis is in a blend with IAGOS aircraft profile

288 measurements within a lower FT pressure-defined region ("FTp" = 300-700 hPa, HEGIFTOM-1).

289 Calculations in the FTp segment are designed to add more samples within the SHADOZ-labeled

290 combination sites (compare profile numbers in **Tables 2 and 3**) and to augment regional trends in

291 HEGIFTOM-2 where no results are reported for the equatorial Americas, Atlantic Ocean or African

292 continent. In defining regions for merging SHADOZ and IAGOS observations, we follow locations

293   presented by Tsivlidou et al. (2023). Profiles from the SHADOZ Quito station (2014-2023) and two

294   IAGOS airports (Bogotá and Caracas) are added to the SHADOZ SC-Para profiles to define the equatorial

295   Americas for determining trends within the FTp (**Table 3**). Also, for the SHADOZ-IAGOS calculations,

296   sonde profiles from the Natal-Ascension pair are combined with 13 airports in west Africa (**Table 3**) to

297   determine trends for a region designated "Atlantic+West Africa," as shown in **Fig. 1b** (color-coded

298   circles) and the second column of **Table 3.** In "East Africa" Nairobi sonde data are combined with IAGOS

299   Nairobi and Addis Ababa ozone profiles. The FTp-designated Equatorial SE Asia consists of KL-Java

300   profiles from SHADOZ combined with IAGOS landing and takeoff data from Kuala Lumpur and

301   Singapore. Time-series of ozone column amounts (in DU and as anomalies) for SHADOZ stations and

302   airports for these 4 "regional" sites appear in **Fig. 3**. The coordinates of individual SHADOZ stations used

303   in the blended dataset (italicized) with IAGOS airports appear in **Table 1**. Calculations with FTp retain

304   Samoa as a single station.

305   **2.1.3 OMI/MLS satellite and sonde total ozone columns**

306   Trends computed with MLR for sonde-derived total tropospheric ozone columns (TrCO) are based on

307   integrating ozone mixing ratios from the surface to the thermal lapse-rate tropopause derived from the

308   radiosondes that accompany each ozonesonde launch. The standard WMO definition of tropopause is

309   used. For the 5 equatorial sites in our analyses, the tropopause is typically between 16 and 17 km. Our

310   $TrCO_{sonde}$ columns and trends are compared to $TrCO_{satellite}$, the tropospheric ozone columns estimated

311   from the OMI/MLS residual as described by Ziemke et al. (2019; updated in the TOAR II paper by Gaudel

312   et al., 2024). These newest OMI/MLR TrCO estimates have been corrected for a ~1%/decade upward

313   drift in OMI over the past two decades (Gaudel et al., 2024; SI material). The OMI/MLS column ozone

314   product is available starting in October 2004. We use monthly average TrCO for both sondes and

315   OMI/MLS between January 2005 and December 2023 **Fig. S1** in Supplemental Material. These are

316   identical to the data used in the Gaudel et al. (2024) TOAR II analyses of tropical ozone.

317   **2.2 Trend analyses**

318   **2.2.1 Multiple Linear Regression (MLR) model**

319   As in T21 and S24, the Goddard MLR model (original version Stolarski et al., 1991, updated in Ziemke

320   et al., 2019) is used for analysis of monthly mean ozone amounts. The MLR model includes terms for

321   annual and semi-annual cycles and oscillations prevalent in the tropics: QBO, MEI (Multivariate ENSO

322   Index, v2) and IOD DMI (Indian Ocean Dipole Moment Index; only for KL-Java):

323   $$O_3(t) = A(t) + B(t) + C(t)MEI(t) + D(t)QBO1(t) + E(t)QBO2(t) + F(t)IOD(t) + \varepsilon(t)$$

324   where t is month. The coefficients are as follows: A through F include a constant and periodic

325   components with 12, 6, 4, and 3 month cycles, where A represents the mean monthly seasonal cycle and

326   B represents the month-dependent linear trend. When annual trends are reported, the B term includes

327   only the 12-month component to generate a single trend value over the period of computation. The

328   model includes data from the MEIv2 (https://www.esrl.noaa.gov/psd/enso/mei/), the two leading QBO

329   EOFs from Singapore monthly mean zonal radiosonde winds at 10, 15, 20, 30, 40, 50, and 70 hPa levels,

330   and IOD DMI (https://psl.noaa.gov/gcos_wgsp/Timeseries/Data/dmi.had.long.data). The ε(t) is the

331   residual, i.e., the difference between the best-fit model and the raw data. T21 noted that the monthly

332   ozone data and MLR model fits for the mid FT (5-10 km) and LMS layers are well-correlated. For the

333   LMS, for example, the correlation coefficients are r = 0.83-0.90 (**Fig. S7** in T21). The IOD DMI term is

334   included for KL-Java, the only station where the IOD impact on the ozone trend is reliably detected.

335   The 95% confidence intervals and p-values for each term in the MLR model as presented here are

336   determined using a moving-block bootstrap technique (10,000 resamples) in order to account for auto-

337   correlation in the ozone time series (Wilks, 1997). The model is applied to ozone anomalies in all cases

338   in order to minimize biases that might arise from intersite ozone differences between pairs for the

339   combined stations: SC-Para, Nat-Asc, KL-Java (**Table 2**). In other words, we calculate ozone anomalies

340   from the individual station's monthly climatology for all profiles before combining the pairs into

341   monthly means and computing the MLR ozone trends. Anomalies are also analyzed for the Nairobi and

342   Samoa station data, although this would be no different than computing MLR trends on the actual ozone

343   timeseries themselves. The MLR model was separately applied to the monthly mean ozone profile

344   anomalies at 100 m resolution, and the monthly mean partial column ozone anomaly amounts from 5-

345   10 km, 10-15 km, and 15-20 km. The MLR model was also applied to the monthly mean tropopause

346   height (TH) anomaly at each station, defined as the 380 K potential temperature surface (e.g., Wargan et

347   al., 2018). Because TH and LMS ozone trends turn out to be strongly correlated (T21), the MLR analysis

348   was also performed for the ozone column amount anomalies referenced to the tropopause. In that case

349   LMS ozone trends refer to changes in the 5 km above the tropopause with the FT extending from the

350   tropopause to 5 km below the tropopause (**Section 3, Table 2**). Finally, the MLR model was applied to

351   total tropospheric column amounts from the sondes ($TrCO_{sonde}$) and corresponding $TrCO_{satellite}$ from

352   OMI/MLS (surface to Tp in **Table 2)**.

353   Note that recent ozone trend studies and the TOAR II guidelines (Chang et al., 2020; Cooper et al.,

354   2020; Chang et al., 2023) have discouraged the use of nomenclature associated with statistical

355   significance whereas the Figures and Tables presented here refer to trends using terminology of 95%

356   confidence intervals (equivalent to p-value < 0.05), the most reliable results in **Section 3** (bold in

357   **Tables 2, 3** and **4)** are explicitly stated as based on p-values < 0.05.

358   Several studies of tropospheric ozone observations have noted a persistence of COVID-19

359   perturbations on ozone trends after 2019 (Ziemke et al., 2022; HEGIFTOM-1; HEGIFTOM-2). A

360   comparison of the extended SHADOZ mean ozone trends (1998-2023) relative to those from T21

361   (covering 1998 to 2019), both summarized in **Table 2,** represents the impact of COVID-19 in the deep

362   tropics. Likewise, SHADOZ was initiated at the end of the powerful 1997-1998 ENSO. Accordingly, we

363 applied MLR to the same 5 sites for 2000-2023 to evaluate any artifacts relative to the 1998 to 2023

364 trends. Those results also appear in **Table 2.**

365 **2.2 Quantile Regression (QR) model**

366 Whereas MLR has been the standard tool for analyzing global total and stratospheric ozone trends, the

367 latter often with satellite data where zonal means can be used, the TOAR II project has recommended

368 using QR as better suited for ozone trends in the troposphere where, for example, urban concentrations

369 can vary by factors of 3-4. Because it is a percentile-based method (Koenker, 2005), the heterogeneously

370 distributed changes of trends can be estimated, as shown, for example, in Gaudel et al. (2020). To date

371 the TOAR II HEGIFTOM trends studies for observations at individual sites (HEGIFTOM-1) and regionally

372 organized data (HEGIFTOM-2) have been studied with the QR approach. In those studies and for the 13

373 individual SHADOZ time-series (**Table 4**) QR has been applied to the median change of the trends,

374 which is equivalent to the least absolute deviation estimator (i.e. aiming to minimize mean absolute

375 deviation for residuals; Chang et al., 2021). The rationale is that compared to least-squares criterion, a

376 median-based approach is more robust when extreme values or outliers are present. Median trends are

377 estimated based on the following multivariate linear model:

378 Observations[t] = a0 + a1*sin(Month*2π/12) + a2*cos(Month*2π/12)

379 + a3*sin(Month*2π/6) + a4*cos(Month*2π/6) + b*t + c*ENSO[t] + N[t],   Eq. 1

380 where harmonic functions are used to represent the seasonality, a0 is the intercept, b is the trend value,

381 c is the regression coefficient for ENSO, and N[t] represents the residuals. Autocorrelation is accounted

382 for by using the moving block bootstrap algorithm, and the implementation details are provided in the

383 TOAR statistical guidelines (Chang et al., 2023). In the individual site analyses of HEGIFTOM

384 observations (HEGIFTOM-1), where all individual ozone records (designated as L1) and monthly means

385 (denoted as L3) were analyzed, annually averaged trends turned out to be the same within

386 uncertainties. Where QR is applied in the present study, L1 ozone data are used.

387 **2.2.3 Trend Sensitivity Studies**

388 Three sensitivity studies were conducted, related to (1) sampling frequency; (2) the complementarity

389 of MLR and QR methods; (3) duration of time-series.

390 A number of TOAR-related studies (Chang et al., 2020; Chang et al., 2021; Chang et al., 2023) have

391 emphasized links between ozone time-series sampling characteristics, i.e., frequency of profile

392 measurements and/or temporal gaps, and trend uncertainty. Gaudel et al. (2024), for example, show

393 uncertainty (as 2-sigma) in median tropospheric ozone profiles; the inference is that 6-15 monthly

394 samples are required for meaningful FT trends (Fig. 1-2 in Supplemental Material, Gaudel et al., 2024).

395 For the first sensitivity test we examined trends dependence on sample size by comparing the annual

396 trends computed with MLR for the lower-mid-FT ozone segment (5-10 km) to the trends from the

397 combined SHADOZ-IAGOS merged monthly mean SHADOZ profiles (L3, 700-300 hPa) for 1998-2023. A

comparison of **Tables 2** and **3** indicate that for the equatorial Americas and Atlantic regions, the sample numbers are increased more than a factor of 2; the other two sites have enhancements of 1.3 and 1.5. The results in DU/decade and %/decade, appear in **Table 3.**

In the second sensitivity study three calculations were made using the data from all individual SHADOZ stations as in HEGIFTOM-1, not only the 5-site equatorial profiles (**Table 2)**. The individual station results appear in **Table 4.** The trend (1998-2023) in mean tropospheric column, TrCO (in DU/decade), was computed using the QR method applied to all profiles at each station (L1, level 1 data) with median (50%-ile) trends shown. The L1 sample numbers ranged from 326 (Watukosek) to 1142 (Hilo); the L1/L3 sample size ratios ranged from 2.2 to 4.3 with only 3 of 13 stations having a ratio below 3.2 (i.e., fewer than 3 profiles per month). These trends can be compared to the MLR trends in **Table 2.** The second calculation was a computation of trends at each station for the FTp column amount used in HEGIFTOM-1(700-300 hPa, comparable to our 5-10 km segment in **Table 2** and the combined IAGOS+SHADOZ FTp columns in **Table 3**). HEGIFTOM-1 pointed out the complementarity of applying both MLR and QR to the 23-yr time-series of mean ozone column amounts. The advantage of MLR is a graphical display of monthly trends that indicate important ways ozone interacts with seasonally varying dynamics, as in S24 or Millet et al. (2025). QR distinguishes trends among different segments of the distribution, an advantage for stations where tropospheric ozone segments are highly variable. To demonstrate this, the QR method (including trends for the 5%-ile, 25%-ile, 75%-ile, 95%-iles) was applied to IAGOS+SHADOZ combined FT dataset for the four regions: equatorial Americas; Atlantic+West Africa; East Africa; equatorial southeast Asia.

The third sensitivity test investigates the degree to which trends and uncertainties depend on the length of sampling. This issue arises because the most frequently used satellite estimates of tropospheric ozone begin after 2003 compared to SHADOZ (1998-) and IAGOS (1994-). The Boynard et al. (2025) study uses IASI products for 2008-2019 (and 2008-2023), comparing only 7 of ~40 potential ozonesonde stations for evaluation. Using L1 mean TrCO tropospheric columns, the QR method was applied to the 13 SHADOZ stations for a 12-year period (2008-2019) for comparison. The results in **Table 5** demonstrate the impact of sampling in a shortened time series.

3 Results and Discussion

3.1 Monthly and seasonal ozone climatology at 5 SHADOZ sites

Figure 4 displays the 5-site monthly ozone climatology based on SHADOZ monthly averaged data from the surface to 20 km. Regional differences in vertical structure within the FT are pronounced. For example, the contours representing the 60-90 ppbv range (yellow to red colors) are abseent in mid-FT ozone over KL-Java or Samoa (**Figs. 4d,e**). Conversely, FT ozone values $\leq$ 30 ppbv (darkest blue shades) observed over KL-Java and Samoa in the middle FT never appear over the other 3 stations: equatorial

Americas (SC-Para, **Fig. 4a**), Nat-Asc or Nairobi (**Figs. 4b,c**). These contrasts may reflect regional

differences in ascending vs. descending nodes of the Walker circulation. The latter feature is partly

responsible for the tropospheric zonal wave-one (Thompson et al., 2003) that refers to a mean TrCO

over the south tropical Atlantic Ocean that is sometimes twice as large as over the western Pacific. There

is less regional variability in LMS ozone. At all stations (**Fig. 4**) above ~16 km the colors and contours

are nearly uniform over the year. Mixing ratio contours of 100 ppbv and 200 ppbv may appear as a thick

white line. The 100 ppbv level is sometimes referred to an ozonopause; typically it is within 1-2 km of

the thermal lapse-rate tropopause.

3.2 FT and LMS ozone annual cycle (1998-2023)

The annual cycle of ozone at the two FT layers and for LMS ozone appear as anomalies in **Fig. 5.** FT

ozone seasonality (**Figs. 5a,b**) is less uniform than for LMS ozone (**Fig. 5c**) and tropopause height (TH,

Fig. 5d). Randel et al. (2007) showed that the near-uniform LMS ozone seasonality in the equatorial

zone is due to the Brewer-Dobson circulation. The more varied FT ozone cycles in **Figs. 5a,b** are due to a

range of different dynamical and chemical influences across the stations. As expected, the annual cycles

for the pressure- and regionally defined FTp ozone (**Fig. 6** in %**)** resemble those for the corresponding

SHADOZ sites in the lower (5-10 km) FT layer in **Fig. 5a**; the magnitudes are similar as well although

Figs. 5 and **6** are illustrated with different scales. In both cases it is seen that there are two seasonal

maxima and minima for KL-Java (**Fig. 5a)** and equatorial SE Asia (**Fig. 6a**). The early year minima are

associated with intense convective activity (T21, S24) that repeats in August at the onset of the Asian

monsoon. KL and Watukosek are also affected by seasonal fire activity at the latter end of the rainy

seasons. These features were described in detail in Stauffer et al. (2018) using Self-Organizing Map

clusters and proxies for convection and fires.

3.3 FT ozone trends: regional and seasonal variability

3.3.1 Trends for 1998-2023

In **Fig. 7** the trends in %/decade computed with MLR at 100-m intervals, for 1998 to 2023, are

displayed (update of Fig. 6 in T21 for the 1998-2019 trends). Changes in the ozone column amounts for

1998-2023 computed from the model (DU/decade and %/decade) for the two FT layers (5-10 km, 10-

15 km) appear in **Fig. 8**. A summary of values for the two layers (and for LMS ozone) appears in **Table

2.** The percentage values in **Fig. 7** and **Table 2** are the result of dividing the MLR B(t) term by the A(t)

annual cycle of ozone term (Section 2.2.1). The MLR-calculated A(t) annual cycle derived from monthly

mean ozone profiles (i.e., no anomaly calculation) is used to convert the B(t) trend in ppmv/decade

(profiles) or DU/decade (partial columns) to %/decade. Ozone trends for both percent/decade and

DU/decade are given in **Table 2.** Shades of red (blue) in **Fig. 7** represent ozone increases (decreases);

cyan hatching denotes trends with p-values < 0.05. The annual mean trends in **Table 2** are computed by

468   taking the average of the 12 monthly trends in DU and dividing by the mean seasonal ozone in DU to

469   yield the annual percentage trend.

470   For 3 of 5 stations in **Figs. 8a** and **c**, there is a pattern of ozone increase at both FT layers in January

471   to April. Percentage-wise the greatest increases are at KL-Java and Nairobi, ~(10-15)%/decade in March

472   and April. However, SC-Para and Samoa at 5-10 km (**Fig. 8a**) exhibit almost no trend at any time of

473   year; at 10-15 km SC-Para and Nairobi show losses up to 10%/decade in February and (5-10)%/decade

474   losses in August and September. However, **Table 2** displays no trend on an annual basis for SC-Para and

475   Nairobi. Inspection of **Fig. 7** suggests small FT trends at Nat-Asc; **Table 2** displays a +3.4%/decade

476   increase in the 10-15 km layer from 1998-2023. The total column, integrated to the tropopause, TrCO,

477   over Nat-Asc, has increased (1.9+ 1.8)%/decade, p<0.05. There are no other annually averaged trends in

478   the FT layers but TrCO for KL-Java (KL-Watukosek in **Table 2**), also increased, (2.6+ 2.3)%/decade.

479   **3.3.2 FT ozone trends sensitivity to COVID-19 and 1997-1998 ENSO**

480   A comparison of the **Table 2** columns for 1998-2023 relative to those for 1998-2019 (the latter is from

481   T21) reveals little. Only the 10-15 km layer at Nat-Asc has entries with p<0.05 for both periods. The

482   extra 4 years reduced the positive trend slightly. This is consistent with studies that found lingering

483   COVID-related declines in sondes and satellites (Ziemke et al., 2022; HEGIFTOM-1). In **Table 2** columns

484   for trends for 2000-2023 can be compared to those for 1998-2023. There is little information in the

485   2000-2023 column, i.e., no trends anywhere except for the TrCO for KL-Java, an area that was well-

486   studied with satellite and some sonde measurements for the period affected by the large ENSO,

487   amplified by the Indian Ocean Dipole pattern (Thompson et al., 2001). After August 1997, as a result of

488   exceptionally high fire activity, ozone increased greatly. That could have meant a smaller change

489   between ozone levels from 1998 through 2023 which would be consistent with a larger, more robust

490   trend for 2000-2023 (4.6%/decade for KL-Java) compared to T21, 2.6%/decade (both p<0.05). Similar

491   trend differences for Kuala Lumpur are also observed with the QR trends in HEGIFTOM-1 (~4-

492   5%/decade for 2000-2022) versus 2.7%/decade in **Table 4**.

493

494   **3.4 LMS ozone trends and mean vertical trend over 5 SHADOZ sites**

495   In T21 (Figs. 10 and 11) trends in the LMS (nominally 15-20 km) showed 5-10%/decade decreases for

496   Nat-Asc, KL-Java and SC-Para between July and October. For the same months those locations exhibited

497   a tropopause increase ~100 m/decade, suggesting that the seasonal ozone increase is an artifact of a

498   changing tropopause. In other words, if the TH increased more air with relatively lower ozone would be

499   located in the 15-20 km layer. We tested this hypothesis by recomputing ozone column changes

500   referenced to the TH for 1998-2019, i.e., evaluating trends in a 5-km thick layer above the TH. The result

501   was that the apparent loss of LMS ozone from July to September or October disappeared. The same

502 analyses performed with LMS ozone and TH for the 1998-2023 period (**Fig. 9)** are the same as for 1998-
503 2019 (T21).
504 Whatever the cause(s) of ozone loss in the LMS, it is a feature clearly captured by SHADOZ data as seen
505 in annually averaged ozone trends derived from the analyses displayed in **Fig. 10.** At 18 km the
506 composite trend from the 8 SHADOZ stations analyzed with MLR is (-4±3)%/decade. The mean trend
507 from ~13 to 3 km is zero, albeit with a ±2σ (95%) ±%/decade. Only below ~2km is the mean ozone
508 trend clearly positive. Most of that increase originates from near-surface pollution over equatorial SE
509 Asia (Fig. 6 in S24).

3.5 Sensitivity tests. Trends method. FT sample numbers. Length of time-series

3.5.1 Complementarity of Trends Methods

512 In Table 4 the median (50%-ile) QR trends from 1998-2023 for the TrCO and FTp ozone segments for
513 the 13 individual SHADOZ stations are presented. The trends for the tropical stations are comparable to
514 the MLR trends in Table 2 and 3, respectively, within their uncertainties, reaffirming the important
515 HEGIFTOM-1 conclusion, i.e., MLR and QR trends from ground-based data (FTIR and Umkehr, as well as
516 sondes) are essentially the same. In **Fig. 11** the timeseries and histograms show the distribution of
517 IAGOS+SHADOZ ozone anomalies (in DU) for the four regions. The median trends from 1998 to 2023
518 (50%-ile) for the FTp ozone segments are also displayed with the lowest and highest (5%, 95%,
519 respectively), 25%-ile and 75%-ile quantiles with red circles denoting p< 0.10. The medians are
520 statistically nearly the same, although as expected, the 2-σ uncertainty bars are smaller with the QR
521 method than with MLR. The MLR trends are higher in all cases except the equatorial Americas (**Fig.
522 11a**). In the latter case, the positive anomalies have increased significantly for the 5% and 25%
523 quantiles over the 26-yr period with no change for the 50%, 75% or 95% quantiles. This signifies that
524 the background (lowest-ozone) air has increasing ozone but the highest-ozone distribution has not
525 changed. Over the Atlantic+West Africa (**Fig. 11b)** there are also small increases in the lowest part of the
526 distribution but the median and higher %iles show no change. Note Natal alone (when not combined
527 with other stations) shows high confidence increases in FTp (and TrCO) ozone (**Table 4**). East Africa
528 (**Fig. 11c)** shows marked increases in the lowest-ozone quantiles and the median but a significant
529 decrease in the highest-ozone (more polluted) air. The opposite is true over equatorial southeast Asia
530 (**Fig. 11d**). The most polluted air corresponds to ozone increasing but the background (lowest ozone)
531 FT segment shows an ozone decrease.

3.5.2 FT sample numbers

533 **Figure 12** monthly ozone trends are based on a total of 1.8 times the number of profiles as those in
534 the other lower FT layer, **Fig. 8a** and **8b.** For the equatorial Americas (blue) twice as many profiles
535 contribute to the trends in **Fig. 12** than in **Figs. 8a** and **8b;** for the Atlantic+West Africa includes 2.5
536 times more profiles than in **Figs. 8a** and **8b.** In all four regions, the seasonality of the trends is nearly the

same between the 5-10 km FT segment (**Figs. 8a** and **8b**) and the corresponding SHADOZ+ IAGOS trend **(Fig. 12).** Furthermore, month by month, the trends are similar to those in the 5-10 km layer in both magnitude and confidence level (uncertainty). **Table 3** shows no trends (p<0.05) at any location. The null trends are illustrated in the annual means at the right of each image in **Figs. 8** and **12**. This was unexpected given the Chang et al. (2023) and Gaudel et al. (2024) suggestions that the uncertainty should decline with more samples and positive trends might be amplified.

3.5.3   Length of time-series

Table 5 displays a comparison of TrOC trends determined by QR for the SHADOZ 26-yr period, 1998-2023 for 13 individual SHADOZ stations, and for the same time-series only between 2008 and 2019. The uncertainties (expressed as ±2-σ) increased by factors of 2-3 or more for 10 of 13 stations. These results are based on a Comment on Boynard et al. (2025) that also compared the time-series changes for 17 mid-latitude ozonesonde stations. Similar uncertainty increases were noted for all 27 stations. Of that total, 9 stations exhibited ozone trend sign changes with the 12-year time-series although only 10 trends were statistically significant. In **Table 5** 2 stations change sign in their trends, 3 stations have a change in confidence level (p<0.05); note that 8 of 13 stations exhibit a substantial change in their trend value, e.g., Samoa, Ascension Island. These results reinforce the need for multi-decade time-series.

3.6 Total tropospheric ozone trends, TrCO (1998-2023), from OMI/MLS and SHADOZ

Trends for the most recent version of OMI/MLS TrCO$_{satellite}$ are based on monthly mean satellite data and determined with MLR over the period 2005 through 2023. Trends for total tropospheric column ozone (TrCO$_{sonde}$) at the 5 SHADOZ sites for the same period appear in circles on the map in **Fig. 13** where the stippling indicates no trend can be determined. For both OMI/MLS and the sondes (**Fig. 7**) shades of red indicate total column ozone increases; blue represents declining ozone over the period of analysis. The mean annual TrCO$_{sonde}$ trends appear in the two rightmost columns in **Tables 2** and **6.** In **Fig. 13** OMI/MLS shows trends > 1 DU/decade (typically 2-9%/decade) only appear over equatorial SE Asia and parts of South America and the eastern Pacific at ~5N latitude. Circles indicate locations and trends for the individual SHADOZ stations. The SHADOZ trends display lower trends than OMI/MLS. On a month-by-month basis, the sonde and OMI/MLS trends are compared in **Fig. 14.** In 3 cases the seasonality of TrCO trends from sonde and OMI/MLS are similar and the annually averaged OMI/MLS TrCO$_{satellite}$ trends are not different from zero (symbols at right of each image). The seasonality of the KL-Java monthly trends agrees well with OMI/MLS; the satellite mean is +5%/decade, gray in **Fig. 14d**. The sonde SC-Para trend (**Fig. 14a**) is quite a bit lower early in the year than the OMI/MLS trends over San Cristóbal and Paramaribo that average +(2-3)%/decade. The Samoa sonde trend and OMI/MLS TrCO trends diverge most of the year. The satellite annual trend is close to +10%/decade, an outlier globally (HEGIFTOM-1) as well as over the tropics where no ground-based study results in a significant trend for TrCO$_{sonde}$ over Samoa (**Section 4.2**).

4 Summary and Conclusions

We have presented a two-part evaluation of tropical ozone trends using a 26-yr record of ozonesonde (SHADOZ, 1998-2023) profiles with selected FT aircraft (IAGOS) ozone data and the most recent OMI/MLS estimates of tropospheric column ozone for 2005-2023. The next section summarizes the findings. It is followed by **Section 4.2** which compares our trends to related TOAR II studies. **Section 4.3** concludes with a consensus view of FT ozone trends and perspectives relevant to the overall TOAR-II climate and tropical assessments.

4.1 Summary of findings

The first part of the study updates trends in FT and LMS ozone for 5 stations, Nairobi, Samoa and three combination sites (San Cristóbal-Paramaribo, Natal-Ascension, Kuala Lumpur-Watukosek) extending the T21 trends, that covered 1998-2019, by 4 years. The new analysis added monthly averaged data from 2000 to 2023 to the Goddard MLR model with standard proxies. Trends in FT (5-10km, 10-15 km) and LMS (15-20 km) layers are illustrated with monthly means and annually averaged changes in DU/decade and %/decade. Trends determined for the period 2000-2023 assessed impacts of the 1997-1998 ENSO on a possible anomalous starting point. Comparisons of trends for the monthly averaged Aura-derived OMI/MLS total tropospheric column ozone product ($TrCO_{satellite}$) were made to those from monthly sonde-derived $TrCO_{sonde}$ for 8 equatorial SHADOZ stations. The principal results of the SHADOZ trend updates and comparisons are as follows:

- The overall characteristics of T21 trends in the FT and LMS are confirmed with 4 additional years of SHADOZ observations. From 1998 to 2023, regional and seasonal variability remains pronounced with FT ozone increasing in thin layers at 4 of 5 SHADOZ stations ~(5-20)%/decade, mostly between January and May. The exception is at SC-Para where there was a 5-10% ozone decrease between 10-15 km during 1998 to 2023 compared 5-10%/decade increases in 1998-2019 (T21). For 1998-2023, the greatest ozone increases occur in multiple layers below 10 km over Nairobi and KL-Java and between 10-15 km over Samoa. However, these features do not translate into annually averaged trends ($p < 0.05$) in the 5-10 km or 10-15 km segments except over Nat-Asc, i.e., adding 4 years of data to equatorial SHADOZ data does not modify the T21 picture of little or no FT ozone change. Only when the total tropospheric column ($TrCO_{sonde}$) trend is evaluated do Nat-Asc (1.9±1.8)%/decade and KL-Java (2.6±2.3)%/decade exhibit the slightest trend ($p < 0.05$). Examining the 5-station average in vertical form shows a null trend from ~3 to 17 km (0±2% within 2σ up to 7 km and ~0±3% from 7 to 17 km). The marginal overall mean increase, +5%/decade below 3 km, is primarily driven by KL-Java changes.

- With the starting year delayed to 2000, the $TrCO_{sonde}$ KL-Java trend (2000-2023) is almost twice as large as for 1998-2023, indicating an effect of the 1997-1998 ENSO on equatorial SE Asia. This is not surprising. Watukosek soundings (1997-1998) show ENSO-induced anomalously high

607 ozone over Indonesia that was also captured by satellite tropospheric ozone estimates from

608 TOMS (Thompson et al., 2001).

609 • The T21 LMS ozone and TH trends are also confirmed with 4 more years of data. For the layer 15-

610 20 km, ozone losses ~5%/decade from June through October, on average, give an all-site average

611 of -3%/decade at 17.5 km, a value similar to satellite averages (Godin-Beekmann et al., 2022). As

612 in T21, re-determining the LMS trends for an ozone column 5 km above the tropopause from

613 1998 to 2023, causes the trend to disappear.

614 • Annually-averaged trends, 2005-2023, determined with MLR for OMI/MLS columns, $TrCO_{satellite}$,

615 over the 8 individual equatorial SHADOZ stations (members of the 5 combined sites) and

616 $TrCO_{sonde}$ overlap within the uncertainties of each. Trends are close to zero at Nat-Asc, Nairobi

617 and KL-Java. The OMI/MLS $TrCO_{satellite}$ trends are marginally positive at SC-Para, with monthly

618 cycles diverging in the early part of the year at SC-Para. OMI/MLS trends do not capture large

619 monthly seasonal variations seen in SHADOZ profiles, especially for negative trends. The large

620 positive trend from OMI/MLS over Samoa does not align with determinations of FT ozone from

621 this or other studies (see below).

622 The second part of the investigation was motivated by statistical issues raised in related TOAR II

623 trends analyses. The results of these analyses are summarized:

624 • Trends methods. The relative merits of trends computed with QR and MLR, previously

625 demonstrated in HEGIFTOM-1, were reinforced with analysis of combined FT SHADOZ-IAGOS

626 data. Although median trends are the same, QR uncertainties are smaller. MLR is superior for

627 capturing seasonal influences but QR provides vital information on whether the background, low-

628 ozone or high-ozone (polluted) populations are changing the most.

629 • Sampling frequency. The sensitivity of the 1998 to 2023 FT ozone trends to sample number was

630 explored by using IAGOS profiles to increase the SHADOZ sample size for the equatorial stations

631 by 80% overall, including a doubling over the equatorial Americas and Atlantic regions, then

632 applying MLR. Median trends were nearly unchanged. No FT trends over the 4 regions (plus

633 Samoa) are detected with p<0.05 although uncertainties, expressed in ppbv/decade, improved

634 30% over the equatorial Americas and by ~15% over 3 of the 4 other sites. These results indicate

635 that current SHADOZ sampling with the 3 combined site records is sufficient in this radiatively-

636 important region.

637 Length of trends. These were examined for the individual station $TrCO_{sonde}$ trends by comparing

638 trends for 1998 to 2023 with a 12-year trend (2008-2019), one of two scenarios investigated by

639 Boynard et al. (2025). The uncertainties (as 2-σ limits) increase by a factor of 2-3 for TrCO at 10 of

640 13 SHADOZ stations and some median trends change sign compared to the 26-year trends (**Table**

641 **4**). The next section shows that even 16-year IASI/Metop trends have an unreasonably low bias

642 with respect to SHADOZ, IAGOS and OMI/MLS trends (**Table 6**), reinforcing a need for multi-

643 decade datasets where ozone changes are relatively small.

644

645 **4.2 Comparison of this study to related TOAR-II investigations**

646 How do our tropical tropospheric ozone trends compare to those in other studies that use SHADOZ

647 and IAGOS profiles and/or satellite data? **Table 6** summarizes our results for the FT, UT segments and

648 for TrCO. The FT ozone comparisons are made with Gaudel et al. (2024) and with results for two

649 HEGIFTOM studies (HEGIFTOM-1; HEGIFTOM-2). For UT ozone, SHADOZ trends are compared to those

650 derived from the lowest 3 layers of MLS (Froidevaux et al., 2025; see their Table 2). TrCO trends are

651 taken from the 5 SHADOZ stations, OMI/MLS (this study) and IASI/Metop (Boynard et al., 2025). Note

652 that the latter study only spans 2008-2023, much less than the SHADOZ data but close to the OMI/MLS

653 period, 2005-2023.

654 The tropical trends study of Gaudel et al. (2024) groups SHADOZ and IAGOS profiles somewhat

655 differently from this study and only extends through 2019 (period of trends are shown in the 4th column

656 of **Table 6**). Our trends and those of Gaudel et al. (2024) for FT ozone and TrCO (**Table 6**) for the

657 equatorial Americas are similar although some are insignificant. The equatorial Americas FT ozone

658 trends range from (-0.01%/decade to -3.3%)/decade, For $TrCO_{sonde}$, derived from profiles, the range is (-

659 1.0 to -3.1)%/decade in between the satellite-based trends. They are (3.1±2.5)%/decade for OMI/MLS

660 (2005-2023) and (-4.0±1.0)%/decade for IASI/Metop (2008-2023), an offset of 7.1%/decade for the

661 median trends. Within given uncertainties, IAGOS, IAGOS-SHADOZ-combined and IASI/Metop agree;

662 their trends all slightly negative.

663 For the Atlantic and west Africa regions, the profile-based comparisons differ in station-airport

664 combinations among our study, Gaudel et al. (2024) and the two HEGIFTOM analyses. The FT and TrCO

665 trends among the 4 studies fall in a relatively small range: (-1.3±2.8)%/decade (FT, Gaudel et al, 2024)

666 to (1.9±1.8)%/decade (TrCO, this study). The larger TrCO from the Natal-Ascension combination

667 appears to result from a higher positive trend in the UT (3.4±2.9)%/decade. Because the FT ozone trend

668 of Gaudel et al. (2024) is negative and the Nat-Asc FT ozone trend is positive (**Table 6**), combining

669 western African IAGOS profiles with the Natal and Ascension measurements, reduces the larger area

670 trend compared to the sonde-only FT ozone trend. **Table 6** shows that for all regions the MLS-derived

671 UT ozone trend estimates fall between +3%/decade and +4%/decade (Froidevaux et al. 2025). Only

672 over the Atlantic region do any of the SHADOZ UT ozone trends fall in this range. Overall, the Atlantic

673 and west Africa FT ozone and $TrCO_{sonde}$ trends are nearly zero, in agreement with OMI/MLS

674 (1.3±1.4)%/decade. As for the equatorial Americas, the 2008-2023 trends from IASI/Metop over the

675 Atlantic and west Africa is much lower: (-4.9±2.0)%/decade. Compare to the OMI/MLS trend, the

676 IASI/Metop median trend has a 6.2%/decade low bias. The picture for east Africa (both SHADOZ and

677 IAGOS profiles over Nairobi) is similar to the Atlantic and west Africa. FT ozone, $TrCO_{sonde}$ and OMI/MLS

678 TrCO trends are essentially null but IASI/Metop displays a (-3.6±1.0)%/decade trend.

679   There is more variability in trends among the ground-based studies for the equatorial SE Asia region

680 than the equatorial Americas, Atlantic and Africa, most likely because different combinations of IAGOS

681 profiles and SHADOZ data were used. Supplementing FT KL-Java SHADOZ profiles with IAGOS data

682 (**Tables 3** and **6**) in our study, a 50% increase in sample size, did not change the trend appreciably:

683 (1.0±2.6)%/decade vs (1.6±3.2)%/decade. The corresponding $TrCO_{sonde}$ over KL-Java increased

684 (2.6±2.3)%/decade. S24 computed trends with MLR for KL-Java for 1998-2022: the $TrCO_{sonde}$ was

685 (3.4±2.6)%/decade. Although the trend period only differs by one year, the smaller trend with the extra

686 year in this study (to 2023) might reflect some COVID impact (columns 5 and 7 in **Table 2**). For

687 OMI/MLS TrCO, determined from a mean of changes averaged over 5^ox5^o grid boxes for KL and

688 Watukosek (Java), there was a (5.6±6.0)%/decade, 2005-2023. The latter change is nearly the same as

689 Gaudel et al. (2024) for both FT ozone and OMI/MLS changes over the same interval. There are several

690 reasons for why Gaudel et al. (2024) FT ozone trends in **Table 6** are larger than our SHADOZ-IAGOS FT

691 ozone trends. First, the fusing of SHADOZ and IAGOS profiles in Gaudel et al. (2024) may be more

692 heavily weighted to polluted IAGOS segments than our merging. Second, reprocessed IAGOS profiles

693 have not been rigorously compared to SHADOZ data up to this point; a new evaluation of IAGOS

694 instrumentation in the World Calibration Center for Ozonesondes may facilitate consistent referencing

695 to an absolute ozone standard in the future (Smit et al., 2024; Smit et al., 2025). Third, with the shorter

696 trend period, especially ending in 2019, the data of Gaudel et al. (2024) would not be affected by lower,

697 COVID-pertrubed ozone concentrations in 2020-2023 as some SHADOZ records were (**Table 2**).

698   The HEGIFTOM-1 FT ozone trend (2000-2022) for Kuala Lumpur is nearly identical to the KL-Java

699 trend, 1998-2023: (2.2±3.0)%/decade. In HEGIFTOM-2 (based on SHADOZ KL and IAGOS from several

700 SE Asia airports) FT ozone increases over a longer period (1995-2022) are (6.2±2.2)%/decade. Thus, in

701 general, over SE Asia, as for the equatorial Americas, Atlantic and Africa, the GB and OMI/MLS trends

702 are in reasonable agreement, given some differences in data selection and minor differences in the trend

703 start and end dates: FT and TrCO ozone increases ~+(2-8)%/decade. Likewise, the IASI/Metop trend for

704 TrCO, (0.0±1.4)%/decade over 2008-2023 (Boynard et al., 2025) is an outlier over SE Asia.

705   Nowhere are the satellite data as divergent from the FT sonde trends, near zero change from our

706 study (1998-2023), Gaudel et al. (2024, for 2004-2019) and HEGIFTOM-1 (2000-2022), than at Samoa

707 (**Table 6**). TrCO from the SHADOZ sondes has no significant change: (-1.4 ±4.8)%/decade, this study); (-

708 3.1±5.4)%/decade (Gaudel et al. 2024). However, the OMI/MLS trend for TrCO is (9.1±8.3)%/decade,

709 2005-2023, and IASI/Metop is (-9.0±1.7)%/decade. The large disagreement in trends from sondes and

710 both satellite instruments, the latter with median TrCO trends that are offset by 18% from one another,

711 underscore the need for profile-based tropospheric ozone trends as an unbiased reference.

4.3 Implications of this study for TOAR II and related assessments

How do our findings apply to an overall TOAR II assessment for tropical ozone? First, there is consensus among the four GB studies: this study, Gaudel et al (2024) and the two HEGIFTOM articles (HEGIFTOM-1; HEGIFTOM-2). These results provide well-characterized trends in FT ozone for input to climate models and a reference for evaluating TrCO, total tropospheric column ozone trends from evolving tropospheric ozone satellite products. In short, over the past 20-25 years, except for equatorial SE Asia, tropical FT and total ozone trends are negligible to within ±(1-2)%/decade. For SE Asia both FT and TrCO have increased from ~(2-8)%/decade. Detailed analyses of sonde profiles by S24 suggest that the annually averaged FT ozone trends are (2-3)%/decade. The (5-7)%/decade increases are seasonal in FT ozone. However, for TrCO it is the large ozone increases in the boundary layer found throughout the year that are dominating the total tropospheric column change.

Second, as far as methods of computing trends, we have shown both the similarity of median trends from QR and MLR as relative advantages of each with SHADOZ and combined SHADOZ-IAGOS profile data. HEGIFTOM-1 reached similar conclusions about QR and MLR trends for 34 ozonesonde stations, including 10 from SHADOZ. The complementarity of QR and MLR for trends attribution was also highlighted in HEGIFTOM-1. The HEGIFTOM papers (HEGIFTOM-1, HEGIFTOM-2), with a multi-instrument perspective, show variable trends among 55 global stations, including over western Europe and North America where both positive and negative tropospheric column trends occur within few hundred km. Overall, except for southeast Asia, FT ozone trends from HEGIFTOM are small to moderate and not distinguishable from zero at a number of tropical and extratropical locations.

Third, both HEGIFTOM-1 and this study investigated the matter of sample density in ground-based data, the former by cutting sample size roughly in half for TrCO and our SHADOZ-IAGOS analyses for FT ozone, roughly doubling it. In both studies trend changes determined with MLR were small (a few tenths of a ppbv/decade) and included both increases and decreases (well-illustrated in Fig. S6 in HEGIFTOM-1). Uncertainty changes ranged from 15-30%, usually improving with more sampling. We conclude that arguments for excluding ground-based trends from TOAR II on the basis of sample size have little merit, particularly given ongoing uncertainties and limited record lengths of many satellite products.

Fourth, by reducing the trend period from 26 years to 12 years, we quantified the degradation of too-short trends for the relatively small changes that apply to much of global FT ozone. The length of trends is only one issue for ozone products derived from satellites that have operated less than two decades. Trends based on the lowermost levels of ozone from MLS (Froidevaux et al., 2025) were largely the same at all SHADOZ stations, (3-4)%/decade for the UT) whereas the sonde-derived trends are geographically variable. Only one of 5 tropical regions we analyzed, Atlantic and west Africa, displayed a

746   UT ozone trend in this range. The discrepancies between GB-based trends is not surprising because MLS

747   does not capture observed variability in UT ozone concentrations, up to a factor of 2 between the

748   Atlantic and western Indian Ocean, that is detected by the sondes or uv sensors (Thompson et al., 2003;

749   Thompson et al., 2017). We compared our profile-based trends to two typical satellite products:

750   IASI/Metop and the well-characterized OMI/MLS. With the uncertainty of the satellite trends, OMI/MLS

751   TrCO trends agreed with $TrCO_{sonde}$ trends in 4 of 5 regions. Where sonde-derived trends were near-zero,

752   IASI/Metop trends sometimes agreed well but for equatorial SE Asia the IASI/Metop zero trend clearly

753   underestimated trends relative to those derived from SHADOZ, SHADOZ-IAGOS combined profiles and

754   OMI/MLS. At Samoa IASI/Metop (-9%/decade) and OMI/MLS (+9%/decade) were both in error,

755   displaying much greater disagreement with the sonde-based trend than anywhere else. There is no easy

756   explanation, but the differing wavelengths, vertical sensitivities, and respective biases in the satellite

757   products likely all play a role.

758   The S24 TOAR-II study is a reminder that the near-zero annually averaged FT ozone trends over most

759   of the tropics (**Figs. 8** and **12**) in the tropics may mask strong seasonal trends (T21). S24 linked the

760   strong February-April increase in FT ozone over KL-Java (1998 to 2022) to declining convection with 4

761   proxies, e.g., outgoing long-wave radiation, velocity potential at 200 hPa. A role for changing dynamics

762   must be considered in tropical tropospheric ozone increases; increasing ozone precursor emissions are

763   apparently not the only driver. In a similar manner, decreases observed in LMS ozone appear to be

764   related to tropopause height changes during the 1998 to 2023 period.

765   In summary, our updated results for SHADOZ stations remain the most reliable reference for trends

766   throughout the tropical troposphere and LMS. We provide a definitive standard for evaluating monthly

767   trends and regional variability of satellite-based products and related models being used for tropical

768   ozone trends. Together with the more extensive HEGIFTOM and IAGOS coverage, our SHADOZ analyses

769   lead to a conclusion that the most reliable trends information for TOAR II is based on re-processed GB

770   measurements. However, coverage of the ground-based instruments is uneven and space-based

771   observations are needed for truly global trends. In order for satellite products to mature and for

772   differences among them to be understood, independent ozone data collection, particularly from

773   ozonesondes referenced to an absolute standard are required. As our investigations with the high-

774   resolution SHADOZ profiles have demonstrated, sonde data will remain the gold standard for deriving

775   trends in the FT and LMS, the two most critical regions where ozone interacts with the climate system.

776
777   **Data Availability**
778
779   All datasets used in this study are openly and publicly accessible.
780   V06 SHADOZ data are available at https://doi.org/10.57721/SHADOZ-V06 (NASA Goddard Space Flight Center
781   (GSFC) SHADOZ Team, 2019).
782   IAGOS and SHADOZ HEGIFTOM data are available at: https://hegiftom.meteo.be
783   Trends in table (*.csv) format are available at: https://tropo.gsfc.nasa.gov/shadoz/SHADOZ_PubsList

784 OMI/MLS data are available at https://acd-ext.gsfc.nasa.gov/Data_services/cloud_slice/new_data.html.
785

786 **Acknowledgments**
787 This study benefitted from discussions with Audrey Gaudel and Kai-Lan Chang (CIRES at NOAA/Chemical Sciences
788 Lab); We thank Kai-Lan Chang for the QR code provided for TOAR II. Support is gratefully acknowledged from the
789 NASA Upper Air Research Program (K. W. Jucks, Program Manager), the SAGE III Program (R. Eckman, Manager),
790 and S-NPP and JPSS (J. F. Gleason, Project Scientist). Quito monitoring was conducted from 2014 to 2021
791 with the support of Universidad San Francisco de Quito USFQ and the Vienna Convention Trust Fund.

792
793 **Competing Interests.** All authors declare that we have no competing interests.
794

795 **References**
796
797 Aumann, H. H., Broberg, S., and Manning, E. M., Northward shift and narrowing of the ITCZ in 20 years of AIRS data,
798   J. Geophys. Res. Atmos. 129, e2023JD038723, https://doi.org/10.1029/2023JD038723, 2024.
799 Boynard, A., Wespes, C., Hadji-Lazaro, J., Sinnathamby, S., Hurtmans, D., Coheur, P-F., Doutriaux-Boucher, M.,
800   Onderwaater, J., Steinbrecht, W., Pennington, E. A., Bowman, K., and Clerbaux, C.: Tropospheric Ozone
801   Assessment Report (TOAR): 16-year ozone trends from the IASI climate data record,
802   https://doi.org/10.5194/egusphere-2025-1054, in review, 2025.
803 Cazorla, M.: Ozone structure over the equatorial Andes from balloon-borne observations and zonal connection with
804   two tropical seal level sites, *J. Atmos. Chem.,* 2016. https://doi.org/10.1007/s10874-016-9348-2
805 Cazorla, M., Parra, R., Herrera, E., and da Silva, F. R.: Characterizing ozone throughout the atmospheric column over the
806   tropical Andes from in situ and remote sensing observations. Elementa. 2021
807   https://doi.org/10.1525/elementa.2021.00019, 2021
808 Cazorla, M., and Herrera, E.: An ozonesonde evaluation of spaceborne observations in the Andean tropics. *Scientific*
809   *Reports* **12**, 15942. https://doi.org/10.1038/s41598-022-20303-7, 2022
810 Chang, K.-L., Cooper, O. R., Gaudel, A., Petropavlovskikh, I., and Thouret, V.: Statistical regularization for trend
811   detection: An integrated approach for detecting long-term trends from sparse tropospheric ozone profiles, Atmos.
812   Chem. Phys., 20, 9915-9938, https://doi.org/10.5194/acp-20-9915-2020, 2020
813 Chang, K.-L., Schultz, M.G., Lan, X., McClure-Begley, A., Petropavlovskikh, I., Xu, X., and Ziemke, J.R.: Trend detection of
814   atmospheric time series: Incorporating appropriate uncertainty estimates and handling extreme events. Elem Sci
815   Anth, 9(1), 00035, https://doi.org/10.1525/elementa.2021.00035, 2021.
816 Chang, K. L., Schultz, M. G., Koren, G., and Selke, N.: (2023). Guidance note on best statistical practices for TOAR
817   analyses. https://doi.org/10.48550/arXiv.2304.14236.
818 Christiansen, A., Mickley, L. J., Liu, J., Oman, L. D., and Hu, L.: Multidecadal increases in global tropospheric ozone
819   derived from ozonesonde and surface site observations: can models reproduce ozone trends? Atmos. Chem. Phys.,
820   https://doi.org/10.5194/acp-22-14751-2022, 2022.
821 Cooper, O. R., Schultz, M., G. Schröder, S., Chang, K.-L., Gaudel, A., Carbajal Benítez, G., Cuevas, E., Fröhlich, M., Galbally,
822   I. E., Kubistin, D., Lu, X., McClure-Begley, A., Molloy, S., Nédélec, P., O'Brien, J., Oltmans, S. J., Petropavlovskikh, I.,
823   Ries, L., Senik, I., Sjöberg, K., Solberg, S., Spain, T. G., Spangl, W., Steinbacher, M., Tarasick, D., Thouret, V., and Xu, X.:
824   Multi-decadal surface ozone trends at globally distributed remote locations, Elem Sci Anth, 8(1), p.23. DOI:
825   http://doi.org/10.1525/elementa.420,
826 De Mazière, M., Thompson, A. M., Kurylo, M. J., Wild, J. D., Bernhard, G., Blumenstock, T., Braathen, G. O., Hannigan, J. W.,
827   Lambert, J.-C., Leblanc, T., McGee, T. J., Nedoluha, G., Petropavlovskikh, I., Seckmeyer, G., Simon, P. C., Steinbrecht,
828   W., and Strahan, S. E.: The Network for the Detection of Atmospheric Composition Change (NDACC): history, status
829   and perspectives, Atmos. Chem. Phys., 18, 4935–4964, https://doi.org/10.5194/acp-18-4935-2018, 2018
830 Froidevaux, L., Kinnison, D. E., Gaubert, B., Schwartz, M. J., Livesey, N. J., Read, W. G., Bardeen, C. G., Ziemke, J. R., and
831   Fuller, R. A.: Tropical upper-tropospheric trends in ozone and carbon monoxide (2005–2020): observational and
832   model results, Atmos. Chem., Phys., https://doi.org/10.5194/acp-25-597-2025, 2025
833 Gaudel, A., Cooper, O. R., Ancellet, G., Barret, B., Boynard, A., Burrows, J. P., Clerbaux, C., Coheur, P.-F., Cuesta, J., Cuevas,
834   E., Doniki, S., Dufour, G., Ebojie, F., Foret, G., Garcia, O., Granados Muños, M. J., Hannigan, J. W., Hase, F., Huang, G.,
835   Hassler, B., Hurtmans, D., Jaffe, D., Jones, N., Kalabokas, P., Kerridge, B., Kulawik, S. S., Latter, B., Leblanc, T., Le
836   Flochmoën, E., Lin, W., Liu, J., Liu, X., Mahieu, E., McClure-Begley, A., Neu, J. L., Osman, M., Palm, M., Petetin, H.,
837   Petropavlovskikh, I., Querel, R., Rahpoe, N., Rozanov, A., Schultz, M. G., Schwab, J., Siddans, R., Smale, D.,
838   Steinbacher, M., Tanimoto, H., Tarasick, D. W., Thouret, V., Thompson, A. M., Trickl, T., Weatherhead, E., Wespes, C.,
839   Worden, H. M., Vigouroux, C., Xu, X., Zeng, G., and Ziemke, J.: Tropospheric Ozone Assessment Report: Present-day

840   distribution and trends of tropospheric ozone relevant to climate and global atmospheric chemistry model
841   evaluation, Elem. Sci. Anth., 6, 39, https://doi.org/10.1525/elementa.291, 2018.
842 Gaudel, A., Cooper, O. R., Chang, K-L., Bourgeois, I., Ziemke, J. R., Strode, S. A. Oman, L. D., Sellitto, P., Nedelec, P., Blot, R.,
843   Thouret, V., and Granier, C.: Aircraft observations since the 1990s reveal increases of tropospheric ozone at
844   multiple locations across the Northern Hemisphere, Science Advances, 6, (34), DOI: 10.1126/sciadv.aba8272, 2020
845 Gaudel, A. Bourgeois, I., Li, M., Chang, K.-L., Ziemke, J., Sauvage, R., Stauffer, R. M., Thompson, A. M., Kollonige, D. E.,
846   Smith, N., Hubert, D., Keppens, A., Cuesta, J., Heue, K.-P., Veefkind, P., Aikin, K., Peischl, J., Thompson, C. R., Ryerson,
847   T. B., Frost, G. J., McDonald, B. C., and Cooper, O. R.: Tropical tropospheric ozone distribution and trends from in
848   situ and satellite data, Atmos. Chem. Phys., https://acp.copernicus.org/articles/24/9975/2024, 2024
849 Godin-Beekmann, S., Azouz, N., Sofieva, V. F., Hubert, D., Petropavlovskikh, I., Effertz, P., Ancellet, G., Degenstein, D. A.,
850   Zawada, D., Froidevaux, L., Frith, S., Wild, J., Davis, S., Steinbrecht, W., Leblanc, T., Querel, R., Tourpali, K.,
851   Damadeo, R., Maillard Barras, E., Stübi, R., Vigouroux, C., Arosio, C., Nedoluha, G., Boyd, I., Van Malderen, R.,
852   Mahieu, E., Smale, D., and Sussmann, R.: Updated trends of the stratospheric ozone vertical distribution in the
853   60° S–60° N latitude range based on the LOTUS regression model , Atmos. Chem. Phys., 22, 11657–11673,
854   https://doi.org/10.5194/acp-22-11657-2022, 2022.
855 Keppens, A., Hubert, D., Granville, J., Nath, O., Lambert, J.-L., Wespes, C., Coheur, P.-F., Clerbaux, C., Boynard, A.,
856   Siddans, R., Latter, B., Kerridge, B., Di Pede, S., Veefkind, P., Cuesta, J., Dufour, G., Heue, K.-P., Coldewey-Egbers, M.,
857   Loyola, D., Orfanoz-Cheuquelaf, A., Satheesan, S. M., Eichmann, K.-U., Rozanov, A., Sofieva, V. F., Ziemke, J. R.,
858   Inness, A., Van Malderen, R., and Hoffmann, L., Harmonisation of sixteen tropospheric ozone satellite data
859   records, egusphere-2024-3746, in review, 2025
860 Khalil, M. A. K., Atmospheric Methane: Its Role in the Global Environment, Springer-Verlag, Berlin, Heidelberg,
861   https://doi.org/10.1007/978-3-662-04145-1, 2000.
862 Koenker, R. (2005). Quantile regression, vol. 38, Cambridge University press,
863   https://doi.org/10.1017/CBO9780511754098
864 Lacis, A. A. Wuebbles, D. J., and Logan, J. A., Radiative forcing of climate by changes in the vertical distribution of
865   ozone, , J. Geophys. Res. Atmos. 101, 9971-9982, https://doi.org/10.1029/JD095iD07p09971, 1990
866 Lee, S., Shelow, D. M., Thompson, A. M., and Miller, S. K.: QBO and ENSO variability in temperature and ozone from
867   SHADOZ (1998-2005), J. Geophys. Res. Atmos., 115, D18105, doi: 10.1029/2009JD013320, 2010
868 Millet, T., Bencherif, H., Bègue, N., Portafaix, T., Toihir, A. M., Sivakumar, V., Vaz Peres, L., Fontaine, M., Pazmiño, A.,
869   Metzger, J-M., Stauffer, R. M., Kollonige, D. E., Thompson, A. M., Evidence for subtropical dynamical changes in
870   Réunion ozone trends (1998-2021), https://essopenarchive.org/users/664913/articles/1287997, 2025
871 Müller, K., Tradowsky, J. S., von der Gathen, P., Ritter, C., SharPatris, S., Notholt, J. Rex, M.: Measurement report: The
872   Palau Atmospheric Observatory and its ozonesonde record – continuous monitoring of tropospheric composition
873   and dynamics in the tropical western Pacific, Atmos. Chem. Phys., 24, 2169–2193, https://doi.org/10.5194/ acp-
874   24-2169-2024, 2024
875 Nakano, T., and Morofuji, T.:Development of an automated pump-efficiency measuring system for ozonesondes
876   utilizing an airbag-type flowmeter, Atmos. Meas. Tech., 16, 1583–1595, https://doi.org/10.5194/ amt-16-1583-
877   2023, 2023
878 NASA Goddard Space Flight Center (GSFC) SHADOZ Team: Southern Hemisphere ADditional OZonesondes (SHADOZ)
879   Version 06 (V06) Station Data (Version V06), NASA [data set], https://doi.org/10.57721/SHADOZ-V06, 2019
880 Pennington, E. A., Osterman, G. B., Payne, V. H., Miyazaki, K., Bowman, K. W., and Neu, J. L.: Quantifying biases in
881   TROPESS AIRS, CrIS, and joint AIRS+OMI tropospheric ozone products using ozonesondes,
882   https://doi.org/10.5194/ egusphere-2024-3701, in review, 2025
883 Plumb, A. R.: A "tropical pipe" model of stratospheric transport, J. Geophys. Res. Atmos. 101 (D6), 3957-3972,
884   https://doi.org/10.1029/95JD03002, 1996
885 Pope, R. J., Kerridge, B. J., Siddans, R., Latter, B. G., Chipperfield, M. P., Feng, W., Pimlott, M. A., Dhomse, S. S., Retscher,
886   C., and Rigby, R.: Investigation of spatial and temporal variability in lower tropospheric ozone from RAL Space UV–
887   Vis satellite products, Atmos. Chem. Phys., 23, 14933–14947, https://doi.org/10.5194/acp-23-14933-2023, 2023
888 Randel, W. J., Park, M., and Wu, F.: A large annual cycle in ozone above the tropical tropopause linked to the Brewer–
889   Dobson circulation, J. Atmos. Sci., 64, 4479-4488, doi: 10.1175/2007JAS2409.1, 2007
890 Randel, W. J., and Thompson, A. M.: Interannual variability and trends in tropical ozone derived from SHADOZ
891   ozonesondes and SAGE II satellite data, J. Geophys. Res. Atmos., 116, D07303, doi:10.1029/ 2010JD015195, 2011
892 Schwartzkopf, M. D., and Ramaswamy, V., Radiative forcing due to ozone in the 1980s: Dependence on altitude of
893   ozone change, Geophysical Res. Letters, https://doi.org/10.1029/93GL00209, 1993
894 Smit, H. G. J., Poyraz, D., Van Malderen, R., Thompson, A. M., Tarasick, D. W., Stauffer, R. M., Johnson, B. J., and Kollonige,
895   D. E., New insights from the Jülich Ozone-Sonde Intercomparison Experiments: Calibration functions traceable to
896   one ozone reference instrument, Atmos. Meas. Tech., 17, 73–112, https://doi.org/10.5194/amt-17-73-2024, 2024

897 Smit, H. G. J., Galle, T., Blot, R., Obersteiner, F., Nédélec, P., Zahn, A., Cousin, J-M., Bundke, U., Petzold, A., Thouret, V., and
898   Clark, H., Intercomparison of IAGOS-CORE, IAGOS-CARIBIC and WMO/GAW-WCCOS ozone instruments at the
899   Environmental Simulation Facility at Jülich, Germany, https://doi.org/10.5194/egusphere-2024-3760, 2025
900 Stauffer, R. M., Thompson, A. M., and Witte, J. C.: Characterizing global ozonesonde profile variability from surface to
901   the UT/LS with a clustering technique and MERRA-2 reanalysis, J. Geophys. Res. Atmos., 123, 6213–6229,
902   https://doi.org/10.1029/2018JD028465, 2018
903 Stauffer, R. M., Thompson, A. M., Kollonige, D. E., Witte, J. C., Tarasick, D. W., Davies, J., Vömel, H., Morris, G. A., van
904   Malderen, R., Johnson, B. J., Querel, R. R., Selkirk, H. B., Stübi, R., and Smit, H. G. J.: A post-2013 dropoff in total ozone
905   at a third of global ozonesonde stations: Electrochemical concentration cell instrument artifacts? Geophys. Res.
906   Lett., 47, e2019GL086791. https://doi.org/10.1029/2019GL086791, 2020
907 Stauffer, R. M., Thompson, A. M., Kollonige, D. E., Tarasick, D. W., Van Malderen, R., Smit, H. G. J., Vömel, H., Morris, G.
908   A., Johnson, B. J., Cullis, P. D., Stübi, R., Davies, J., and Yan, M. M.: An examination of the recent stability of
909   ozonesonde global network data, *Earth Space. Sci.,* https://doi.org/10.1029/2022EA002459, 2022
910 Stauffer, R. M., Thompson, A. M., Kollonige, D. E., Komala, N., Khirzin Al-Ghazali, H., Risdianto, D. Y.,Dindang, A., bin
911   Jamaluddin, A. F., Sammathuria, M. K., Zakaria, N. B., Johnson, B. J., and Cullis, P. D., Dynamical drivers of free-
912   tropospheric ozone increases over equatorial Southeast Asia, Atmos. Chem. Phys.,
913   https://doi.org/10.5194/acp-24-5221-2024, 2024
914 Stolarski, R. S., Bloomfield, P. R., McPeters, R. D., and Herman, J. R.: Total ozone trends deduced from Nimbus 7 TOMS
915   data, Geophys. Res. Lett., 18, 1015-1018, https://doi.org/10.1029/91GL01302, 1991
916 Thompson, A. M.: The oxidizing capacity of the Earth's atmosphere: Probably past and future changes, Science,
917   https://doi.org/10.1126/science.256.5060.1157, 1992
918 Thompson, A. M., and Cicerone, R. J.: Atmospheric CH_4, CO, and OH from 1860 1985, Nature, 321, 148 150;
919   https://www.nature.com/articles/321148a0, 1986
920 Thompson, A. M., Huntley, M. A., and Stewart, R. W.: Perturbations to tropospheric oxidants, 1985-2035: 1. Model
921   calculations of ozone and OH in chemically coherent regions, J. Geophys. Res. Atmos.,
922   https://doi.org/10.1029/JD095iD07p09829, 1990
923 Thompson, A. M., Witte, J. C., Hudson, R. D., Guo, H., Herman, J. R., and Fujiwara, M.: Tropical tropospheric ozone and
924   biomass burning, *Science,* 291, 2128-2132, 2001; doi: 10.1126/science.291.5511.2128
925 Thompson, A. M., Witte, J. C., , Oltmans, S. J., Schmidlin, F. J, Logan, J. A., Fujiwara, M., Kirchhoff, V. W. J. H., Posny, F.,
926   Coetzee, G. J. R., Hoegger, B., Kawakami, S., Ogawa, T., Fortuin, J. P. F., and Kelder, H.: Southern Hemisphere
927   ADditional Ozonesondes (SHADOZ) 1998-2000 tropical ozone climatology. 2. Tropospheric variability and the
928   zonal wave-one, J. Geophys. Res. Atmos., 108, 8241, doi: 10.1029/2002JD002241, 2003
929 Thompson, A. M., Witte, J. C., Smit, H. G. J., Oltmans, S. J., Johnson, B. J., Kirchhoff, V. W. J. H., and Schmidlin, F. J.:
930   Southern Hemisphere Additional Ozonesondes (SHADOZ) 1998-2004 tropical ozone climatology. 3.
931   Instrumentation, Station Variability, Evaluation with Simulated Flight Profiles, J. Geophys. Res., 112, D03304, doi:
932   10.1029/ 2005JD007042, 2007
933 Thompson, A. M., Allen, A. L., Lee, S,. Miller, S. K., and Witte, J. C.: Gravity and Rossby wave signatures in the tropical
934   troposphere and lower stratosphere based on Southern Hemisphere Additional Ozonesondes (SHADOZ), 1998–
935   2007*, J. Geophys. Res. Atmos.,* 116, D05302, doi:10.1029/2009JD013429, 2011
936 Thompson, A. M., Miller, S. K., Tilmes, S., Kollonige, D. W., Witte, J. C., Oltmans, S. J., Johnson, B. J., Fujiwara, M.,
937   Schmidlin, F. J., Coetzee, G. J. R., Komala, N., Maata, M.. bt Mohamad, M., Nguyo, J., Mutai, C., Ogino, S.-Y., Raimundo
938   Da Silva, F., Paes Leme, N. M., Posny, Scheele, R., F. Selkirk,' H. B., Shiotani, M., Stübi, R., Levrat, G., Calpini, B.,
939   Thouret, V., Tsuruta, H., Valverde Canossa, J. Vömel, H., Yonemura, S. Andrés Diaz, J., Tan Thanh, N, T., and Thuy Ha,
940   H. T.: Southern Hemisphere Additional Ozonesondes (SHADOZ) ozone climatology (2005-2009): Tropospheric and
941   tropical tropopause layer (TTL) profiles with comparisons to OMI-based ozone products. J. Geophys. Res., **117,**
942   D23301, doi: 10.1029/2010JD016911, 2012
943 Thompson, A. M., Balashov, N.V., Witte, J. C., Coetzee, G. J. R., Thouret, V., and Posny, F.: Tropospheric ozone increases
944   in the southern African region: Bellwether for rapid growth in southern hemisphere pollution? Atmos. Chem.
945   Phys., **14,** 9855-9869, 2014.
946 Thompson, A. M., Witte, J. C., Sterling, C., Jordan, A., Johnson, B. J., Oltmans, S. J., Fujiwara, M., Vömel, H., Allaart, M.,
947   Piters, A., Coetzee, G. J. R., Posny, F., Corrales, E., Andres Diaz, J., Félix, C. Komala, N., Lai N., Maata, M., Mani, F.,
948   Zainal, Z., Ogino, S.-Y., Paredes, F., Luiz Bezerra Penha, T., Raimundo da Silva, F., Sallons-Mitro, F., Selkirk, H. B.,
949   Schmidlin, F. B., Stuebi, R., and Thiongo, K.: First reprocessing of Southern Hemisphere Additional Ozonesondes
950   (SHADOZ) ozone profiles (1998–2016): 2. Comparisons with satellites and ground-based instruments, J. Geophys.
951   Res. Atmos., 122, 13,000–13,025, 2017; https://doi.org/10.1002/2017JD027406
952 Thompson, A. M., Smit, H. G. J., Witte, J. C., Stauffer, R. M., Johnson, B. J., Morris, G. A., von der Gathen, P., Van Malderen,
953   R., Davies, J., Piters, A., Allaart, M., Posny, F., Kivi, R., Cullis, P., Ahn, N. T. H., Corrales, E., Machinini, T., Raimundo

daSilva, F., Paiman, G., Thiong'o, K., Zainal, Z., Brothers, G. B., Wolff, K. R., Nakano, T., Stübi, R., Romanens, G., Coetzee, G. J. R., Diaz, J. A., Mitro, S., 'bt Mohamad, M., and Ogino, S.-Y.: Ozonesonde Quality Assurance: The JOSIE-SHADOZ (2017) Experience, Bull. Am. Meteor. Society, doi.org/10.1175/BAMS-17-0311, 2019

Thompson, A. M., Stauffer, R. M., Wargan, K., Witte, J. C., Kollonige, D. E., and Ziemke, J. R.: Regional and seasonal trends in tropical ozone from SHADOZ profiles: Reference for models and satellite products, J. Geophys. Res Atmos., https://agupubs.onlinelibrary.wiley.com/doi/10.1029/2021JD034691, 2021

Thouret, V., Clark, H., Petzold, A., Nédélec, P., and Zahn, A.:. IAGOS: Monitoring Atmospheric Composition for Air Quality and Climate by Passenger Aircraft. (pp. 1-14). https://doi.org/10.1007/978-981-15-2527-8_57-1, 2022

Tselioudis, G., Remillard, J., Jakob, C., and Rossow, W. B.: Contraction of the world's storm-cloud zones the primary contributor to the 21st century increase in the Earth's sunlight absorption. Geophys. Res., Lett., https://doi.org/10.1029/2025GL114882, 2025

Tsivlidou, M., Sauvage, B., Bennouna, Y., Blot, R., Boulanger, D., Clark, H., Le Flochmoën, E., Nédélec, P., Thouret, V., Wolff, P. & Barret, B.: Tropical tropospheric ozone and carbon monoxide distributions: characteristics, origins, and control factors, as seen by IAGOS and IASI. (Vol. 23, pp. 14039-14063). https://doi.org/10.5194/acp-23-14039-2023, 2023

Van Malderen, R., Thompson, A. M., Kollonige, D. E., Stauffer, R. M., Smit, H. G. J., Maillard Barras, E., Vigouroux, C., Petropavlovskikh, I., Leblanc, T.. Thouret, V., Wolff, P., Effertz, P., Tarasick, D. W., Poyraz, D., Ancellet, G., De Backer, M.-R., Evan, S., Flood, V., Frey, M. M., Hannigan, J. W., Hernandez, J. L., Iarlori, M., Johnson, B. J., Jones, N., Kivi, R., Mahieu, E., McConville, G., Müller, K., Nagahama, T., Notholt, J., Piters, A., Prats, N., Querel, R., Smale, D., Steinbrecht, W., Strong, K., and Sussmann, R.: Global ground-based tropospheric ozone measurements: Reference data and individual site trends (2000–2022) from the TOAR-II/HEGIFTOM Project, Atmos. Chem. Phys. 25, 7187–7225, https://doi.org/10.5194/acp-25-7187-2025, 2025a

Van Malderen, R., Zang, Z., Chang, K.-L., Björklund, R., Cooper, O. R., Liu, J., Barras, E. M., Vigouroux, C., Petropavlovskikh, I., Leblanc, T., Thouret, V., Wolff, P., Effertz, P., Gaudel, A., Tarasick, D. W., Smit, H. G. J., Thompson, A. M., Stauffer, R. M., Kollonige, D. E., Poyraz, D., Ancellet, G., De Backer, M.-R., Frey, M. M., Hannigan, J. W., Hernandez, J. L., Johnson, B. J., Jones, N., Kivi, R., Mahieu, E., Morino, I., McConville, G., Müller, G., Murata, I., Notholt, J., Piters, A., Prignon, M., Querel, R., Rizi, V., Smale, D., Steinbrecht, W., Strong, K., and Sussmann, R.: Global ground-based tropospheric ozone measurements: Regional tropospheric ozone column trends from the TOAR-II/HEGIFTOM homogenized datasets, Atmos. Chem., Phys., DOI: 10.5194/egusphere-2024-3745, in press, 2025b

Wargan, K., Orbe, C., Pawson, S., Ziemke, J. R., Oman, L. D., Olsen, M. A., Coy, L., and Knowland, K. E., Recent decline in extratropical lower stratospheric ozone attributed to circulation changes, Geophysical Research Letters, https://doi.org/10.1029/2018GL077406, 2018

Wilks, D.S. (1997). Resampling hypothesis tests for autocorrelated fields, J. Climate, 10 (1), 65-82, https://doi.org/10.1175/1520-0442(1997)010<0065:RHTFAF>2.0.CO;2

Witte, J. C., Thompson, A. M., Smit, H. G. J., Fujiwara, M., Posny, F., Coetzee, G. J. R., Northam, E. T., Johnson, B. J., Sterling, C. W., Mohammed, M., Ogino, S.-Y., Jordan, A., Raimundo Silva, F., and Zainal, Z.: First reprocessing of Southern Hemisphere ADditional OZonesondes (SHADOZ) profile records (1998-2015) 1: Methodology and evaluation, J. Geophys. Res., 122, 6611-6636, doi: 10.1002/2016JD026403, 2017

Zhang, Y., Cooper, O. R., Gaudel, A., Thompson, A. M., Nédelec, P., Ogino, S.-Y., and West, J. J.: Equatorward redistribution of emissions dominates the 1980 to 2010 tropospheric ozone change, Nature-Geoscience, doi: 10.1038/NGEO2827, 2016

Ziemke, J. R., and Chandra, S.: Madden-Julian Oscillation in tropospheric ozone, J. Geophys. Res. Atmos., https://doi.org/10.1029/2003GL018523, 2003

Ziemke, J. R., Chandra, S., Duncan, B. N., Froidevaux, L., Bhartia, P. K., Levelt, P. F., and Waters, J. W.: Tropospheric ozone determined from Aura OMI and MLS: Evaluation of measurements and comparison with the Global Modeling Initiative's Chemical Transport Model, J. Geophys. Res., 111, D19303, https://doi.org/10.1029/2006JD007089, 2006

Ziemke, J. R., Oman, L. D., Strode, S. A., Douglass, A. R., Olsen, M. A., McPeters, R. D., Bhartia, P. K., L. Froidevaux, L.. Labow, G. J.,. Witte, J. C., Thompson, A. M., D. P. Haffner, D. P., Kramarova, N. A., Frith, S. M., Huang, L. K., Jaross, G. R., Seftor, C. J., Deland, M. T., Taylor, S. L.: Trends in global tropospheric ozone Inferred from a composite record of TOMS/OMI/MLS/OMPS satellite measurements and the MERRA-2 GMI simulation, Atmos. Chem. Phys., 19, 3257–3269, 2019. https://doi.org/10.5194/acp-19-3257-2019, 2019

Ziemke, J. R,, Kramarova, N. A., Frith, S. M., Huang, L. K., Haffner, D., Wargan, K,, Lamsal, L. N., Labow, G. J., Bhartia, P. K.: NASA Satellite Measurements Show Global-Scale Reductions in Free Tropospheric Ozone in 2020 and Again in 2021 During COVID-19, Geophys. Res., Lett. https://doi.org/10.1029/2022GL098712, 2022

Tables and Figures

Table 1. List of the 27 total SHADOZ (italicized) and IAGOS sites, and their metadata, used in

this analysis.

Site	Country	Observation Network	Latitude	Longitude	Altitude (m)
Abidjan (ABJ)	Cote d'Ivoire	IAGOS	5.25	-3.93	6
Accra (ACC)	Ghana	IAGOS	5.61	-0.17	62
Addis Ababa (ADD)	Ethiopia	IAGOS	8.98	38.80	2326
Ascension Island	United Kingdom	SHADOZ	-7.58	-14.24	85
Bogota (BOG)	Colombia	IAGOS	4.70	-74.14	2548
Brazzaville (BZV)	Congo (Brazzaville)	IAGOS	-4.26	15.25	319
Caracas (CCS)	Venezuela	IAGOS	10.60	-67.01	71
Cotonou (COO)	Benin	IAGOS	6.35	2.39	6
Douala (DLA)	Cameroon	IAGOS	4.01	9.72	10
Hanoi	Vietnam	SHADOZ	21.01	105.80	6
Hilo, Hawaii	United States	SHADOZ	19.43	-155.04	11
Irene	South Africa	SHADOZ	-25.90	28.22	1524
Kinshasa (FIH)	Congo (Kinshasa)	IAGOS	-4.39	15.45	313
Koror	Palau	SHADOZ	7.34	134.47	23
Kuala Lumpur	Malaysia	SHADOZ	2.73	101.27	17
Kuala Lumpur (KUL)	Malaysia	IAGOS	2.76	101.71	21
Lagos (LOS)	Nigeria	IAGOS	6.58	3.32	41
Libreville (LBV)	Gabon	IAGOS	0.46	9.41	12
Lome (LFW)	Togo	IAGOS	6.17	1.25	22
Luanda (LAD)	Angola	IAGOS	-8.85	13.23	74
Malabo (SSG)	Equatorial Guinea	IAGOS	3.76	8.72	23
Nairobi	Kenya	SHADOZ	-1.27	36.80	1795
Natal	Brazil	SHADOZ	-5.42	-35.38	42
Pago Pago	American Samoa	SHADOZ	-14.23	-170.56	77
Paramaribo	Surinam	SHADOZ	5.80	-55.21	23
Port Harcourt (PHC)	Nigeria	IAGOS	5.01	6.95	27
Quito	Ecuador	SHADOZ	-0.20	-78.44	2414
Reunion Island	France	SHADOZ	-21.06	55.48	10
San Cristobal	Ecuador	SHADOZ	-0.89	-89.61	8
Sao Paulo (GRU)	Brazil	IAGOS	-23.43	-46.48	750
Singapore (SIN)	Singapore	IAGOS	1.36	103.99	7
Suva	Fiji	SHADOZ	-18.13	178.40	6
Watukosek, Java	Indonesia	SHADOZ	-7.46	112.43	50
Yaounde (NSI)	Cameroon	IAGOS	3.70	11.55	694

Table 2. SHADOZ metadata: number of profiles, annual trends. Each row indicates a different segment: 5-10km, 10-15km, 15-20km, TH-5km to TH, TH to TH +5km, and surface to Tp (tropopause). Periods analyzed (columns) are 1998-2019 (T21), 1998-2023, 2000-2023; 2005-2023 for OMI/MLR comparisons in total tropospheric ozone column amount (TrCO). Annually-averaged MLR partial column ozone linear trends are shown DU per decade and in percent per decade, with the 95% confidence interval. Trends with p-values <0.05 are shown in bold.

SHADOZ T21 Updated MLR FT Ozone Trends										
Station	Altitude Range	Number of Profiles	1998-2019 T21 Annual Trend ± 2*sigma (DU/decade)	1998-2019 T21 Annual Trend ± 2*sigma (%/decade)	1998-2023 Annual Trend ± 2*sigma (DU/decade)	1998-2023 Annual Trend ± 2*sigma (%/decade)	2000-2023 Annual Trend ± 2*sigma (DU/decade)	2000-2023 Annual Trend ± 2*sigma (%/decade)	2005-2023 Annual Trend ± 2*sigma (DU/decade)	2005-2023 Annual Trend ± 2*sigma (%/decade)
San Cristobal – Paramaribo	5-10km	1370	0.2±0.3	1.9±3.1	-0.1±0.3	-0.9±3.7	-0.1±0.3	-1.2±3.8	-0.3±0.5	-3.6±5.1
	10-15km		0.1±0.2	1.5±4.0	-0.2±0.3	-3.5±4.5	-0.2±0.3	-4.0±4.4	**-0.4±0.4**	**-6.6±6.5**
	15-20km		**-0.4±0.4**	**-3.1±2.8**	**-0.5±0.4**	**-3.9±2.9**	-0.4±0.4	-2.8±3.2	-0.4±0.7	-3.3±5.5
	TH-5km to TH		0.0±0.2	0.2±4.2	-0.2±0.3	-2.9±5.1	-0.2±0.3	-2.9±5.2	-0.3±0.4	-5.9±7.5
	TH to TH+5km		0.2±0.6	0.6±2.3	-0.3±0.7	-1.2±2.6	-0.3±0.8	-1.1±2.9	-0.4±1.3	-1.5±4.5
	TrCO, surf-Tp		NA	NA	-0.3±0.9	-1.0±3.3	-0.2±1.0	-0.8±3.6	-0.4±1.6	-1.4±5.9
Natal - Ascension Island	5-10km	1646	0.2±0.3	1.6±2.3	0.2±0.3	1.9±2.2	0.1±0.2	0.5±1.8	0.0±0.4	0.3±2.9
	10-15km		**0.3±0.2**	**3.9±2.8**	**0.2±0.2**	**3.4±2.9**	0.1±0.2	1.7±2.4	0.1±0.3	0.7±3.8
	15-20km		-0.0±0.3	-0.4±2.4	-0.1±0.3	-1.0±2.3	-0.2±0.3	-1.4±2.6	-0.3±0.5	-2.4±3.8
	TH-5km to TH		**0.3±0.2**	**4.7±2.7**	**0.2±0.2**	**3.4±2.9**	0.1±0.2	1.7±2.4	0.0±0.2	0.2±3.3
	TH to TH+5km		0.5±0.5	1.9±1.9	0.2±0.7	0.9±2.7	-0.0±0.6	-0.1±2.5	-0.4±0.9	-1.6±3.7
	TrCO surf-Tp		NA	NA	**0.7±0.6**	**1.9±1.8**	0.3±0.7	0.9±1.9	0.3±1.0	1.0±2.8
Nairobi	5-10km	976	0.1±0.3	1.2±3.1	0.1±0.3	0.5±3.0	0.1±0.4	1.0±3.5	-0.0±0.7	-0.3±6.3
	10-15km		-0.0±0.2	-0.2±3.4	-0.1±0.2	-1.5±3.2	-0.1±0.3	-1.9±4.2	-0.2±0.6	-2.4±8.2
	15-20km		0.1±0.3	0.6±2.5	0.1±0.5	0.9±3.9	0.3±0.5	2.4±4.2	0.7±0.9	5.6±6.9
	TH-5km to TH		0.0±0.2	0.7±3.2	-0.0±0.2	-0.0±2.5	-0.0±0.2	-0.1±3.3	-0.0±0.4	-0.2±6.1
	TH to TH+5km		0.5±0.7	1.9±2.7	0.4±0.9	1.4±3.5	0.5±1.1	1.7±4.2	1.2±1.7	4.5±6.3
	TrCO, Surf-Tp		NA	NA	0.3±0.7	1.1±2.5	0.3±0.9	1.0±3.2	-0.4±1.5	-1.5±5.2
Kuala Lumpur – Watukosek	5-10km	870	0.1±0.2	1.9±3.0	0.1±0.2	1.0±2.5	0.1±0.2	1.0±3.1	-0.1±0.3	-1.2±4.3
	10-15km		-0.0±0.1	-0.6±3.3	0.0±0.1	1.3±3.6	0.1±0.2	2.9±4.2	0.2±0.2	4.3±6.6
	15-20km		**-0.7±0.3**	**-5.8±2.8**	-0.3±0.6	-2.4±4.8	-0.1±0.6	-0.4±5.3	0.6±0.8	5.2±6.8
	TH-5km to TH		-0.1±0.1	-3.2±3.3	0.0±0.2	0.8±5.7	0.1±0.2	2.6±6.8	0.2±0.3	5.1±8.8

Region	Layer	N								
	TH to TH+5km		-0.1±0.8	-0.5±3.0	0.2±1.1	0.9±4.2	0.3±1.2	1.1±4.5	**1.7±1.0**	**7.0±4.0**
	TrCO, surf-Tp		NA	NA	**0.6±0.6**	**2.6±2.3**	**1.1±0.7**	**4.6±2.8**	0.7±1.1	3.0±4.6
Samoa	5-10km	928	0.1±0.3	1.4±4.7	0.1±0.3	0.8±4.4	-0.0±0.3	-0.2±4.5	-0.2±0.4	-3.0±5.7
	10-15km		0.1±0.3	2.5±6.5	-0.0±0.4	-1.3±9.2	-0.1±0.4	-3.0±9.4	**-0.4±0.4**	**-10.0±10.0**
	15-20km		-0.4±0.5	-2.8±3.4	-0.3±0.7	-2.3±5.2	-0.4±0.7	-2.9±5.3	**-1.0±0.8**	**-7.0±5.4**
	TH-5km to TH		0.0±0.3	0.2±6.5	-0.1±0.4	-1.7±8.8	-0.1±0.4	-2.5±9.5	**-0.5±0.4**	**-10.6±9.0**
	TH to TH+5km		-0.3±0.7	-0.9±2.4	-0.4±0.9	-1.4±3.1	-0.9±0.9	-2.9±3.0	**-1.2±1.1**	**-3.9±3.7**
	TrCO, surf-Tp		NA	NA	-0.3±1.0	-1.4±4.8	-0.3±1.1	-1.3±5.4	-0.9±1.4	-4.4±6.5

1021

Table 3. SHADOZ and IAGOS combined MLR ozone trends values for FTp (700-300 hPa) partial column for 5 regions: Equatorial Americas, Atlantic and West Africa, East Africa, Equatorial Southeast Asia, and Samoa (individual record). The individual sites are listed for each region. Annually-averaged MLR partial column ozone linear trends are shown DU per decade and in percent per decade, with the 95% confidence interval. Trends with p-values <0.05 are shown in bold.

SHADOZ MLR Regional FT (700-300 hPa) Ozone Trends				
Region Name	**Individual SHADOZ & IAGOS Locations (IAGOS regions in bold)**	**Number of Profiles**	**1998-2023 Annual Trend ± 2*sigma (DU/decade)**	**1998-2023 Annual Trend ± 2*sigma (%/decade)**
Equatorial Americas	San Cristobal (Ecuador), Paramaribo (Suriname), Quito (Ecuador), Caracas (Venezuela), Bogota (Colombia)	2821	0.00 ± 0.31	-0.01 ± 2.57
Atlantic and West Africa	Natal (Brazil), Ascension Island (UK); **Central Africa** [Luanda (Angola), Brazzaville (Congo), Kinshasa (Democratic Republic of Congo)], **Gulf of Guinea** [Lomé (Togo), Yaoundé (Cameroon), Douala (Cameroon), Libreville (Gabon), Accra (Ghana), Abidjan (Ivory Coast), Malabo (Equatorial Guinea), Cotonou (Benin), Port Harcourt (Nigeria)], **Lagos** (Nigeria)	4271	0.12 ± 0.39	0.69 ± 2.28
East Africa	Nairobi (Kenya), Addis Ababa (Ethiopia)	1297	0.12 ± 0.38	0.85 ± 2.69
Equatorial Southeast Asia	Kuala Lumpur (Malaysia), Watukosek (Indonesia); **Gulf of Thailand** [Kuala Lumpur (Malaysia), Singapore (Singapore)]	1305	0.16 ± 0.34	1.57 ± 3.25
Samoa	Pago Pago (Am. Samoa)	928	-0.04 ± 0.38	-0.42 ± 3.85

Table 4. SHADOZ QR median (50%-ile) annual ozone trends values (1998-2023) for TrCO (surface to tropopause) and FTp (700-300 hPa) columns in DU/decade and in %/decade with ±2*sigma. Trends with p-values <0.05 are shown in bold. L1 data is daily data from the HEGIFTOM database

 (https://hegiftom.meteo.be/datasets). The italicized stations are the subtropical SHADOZ sations,
defined as latitude outside of ±19 degrees.

SHADOZ QR 1998-2023 L1 Annual Ozone Trends							
Station	Latitude	Longitude	L1 Obs #	TrCO (surf-Tp) Trend ± 2*sigma (DU/decade)	TrCO (surf-Tp) Trend ± 2*sigma (%/decade)	FTp (300-700 hPa) Trend ± 2*sigma (DU/decade)	FTp (300-700 hPa) Trend ± 2*sigma (%/decade)
Samoa	-14.23	-170.56	797	-0.29 ± 0.54	-1.41 ± 2.59	-0.04 ±0.36	-0.44 ± 3.58
Hilo	*19.43*	*-155.04*	*1142*	*-0.71 ± 0.72*	*-2.21 ± 2.25*	*-0.20 ± 0.24*	*-1.33 ± 1.51*
San Cristobal	-0.89	-89.61	350	-0.44 ± 1.14	-1.69 ± 4.42	-0.03 ±0.48	-0.24 ± 3.79
Paramaribo	5.80	-55.21	855	0.22 ± 0.62	0.80 ± 2.27	0.09 ± 0.34	0.67 ± 2.62
Natal	-5.42	-35.38	676	**1.04 ± 0.68**	**3.04 ± 2.00**	**0.56 ± 0.48**	**3.29 ± 2.79**
Ascension Island	-7.58	-14.24	676	0.20 ± 0.84	0.53 ± 2.19	0.04 ± 0.40	0.21 ± 2.09
Irene	*-25.90*	*28.22*	*387*	*0.53 ± 0.98*	*1.44 ± 2.63*	*0.38 ± 0.48*	*2.02 ± 2.63*
Nairobi	-1.27	36.80	872	0.26 ± 0.70	0.94 ± 2.53	0.16 ± 0.46	1.11 ± 3.13
Reunion	*-21.06*	*55.48*	*735*	***2.63 ± 0.78***	***7.22 ± 2.14***	***0.90 ± 0.40***	***5.22 ± 2.31***
Kuala Lumpur	2.73	101.27	456	0.67 ± 1.12	2.68 ± 3.69	0.10 ± 0.50	0.95 ± 4.77
Hanoi*	*21.01*	*105.80*	*350*	*1.94 ± 2.18*	*4.85 ± 5.45*	*0.43 ± 0.96*	*2.46 ± 5.52*
Watukosek	-7.46	112.43	326	0.71 ± 1.74	2.87 ± 6.99	0.22 ± 0.78	2.07 ± 7.26
Fiji	-18.13	178.40	391	-0.28 ± 0.84	-1.16 ± 3.54	0.17 ± 0.68	1.48 ± 5.71

* Hanoi dataset starts in 2004 (not 1998).

Table 5. SHADOZ QR median (50%-ile) annual ozone trends values (1998-2023 and 2008-2019) for
TrCO (surface to tropopause) columns in DU/decade with ±2*sigma. Trends with p-values <0.05 are

shown in bold. L1 data is daily data from the HEGIFTOM database
(https://hegiftom.meteo.be/datasets).

SHADOZ QR L1 Annual TrCO Trends for 1998-2023 and 2008-2019				
Station	Latitude	Longitude	1998-2023 TrCO (surf-Tp) Trend ± 2*sigma (DU/decade)	2008-2019 TrCO (surf-Tp) Trend ± 2*sigma (DU/decade)
Samoa	-14.23	-170.56	-0.29 ± 0.54	**-1.74 ± 1.70**
Hilo	19.43	-155.04	**-0.71 ± 0.72**	**-1.46 ± 1.46**
San Cristobal	-0.89	-89.61	-0.44 ± 1.14	-0.39 ± 2.42
Paramaribo	5.80	-55.21	0.22 ± 0.62	0.47 ± 1.26
Natal	-5.42	-35.38	**1.04 ± 0.68**	-1.06 ± 2.06
Ascension Island	-7.58	-14.24	0.20 ± 0.84	1.26 ± 2.04
Irene	-25.90	28.22	0.53 ± 0.98	-1.76 ± 2.74
Nairobi	-1.27	36.80	0.26 ± 0.70	0.39 ± 1.58
Reunion	-21.06	55.48	**2.63 ± 0.78**	1.67 ± 1.92
Kuala Lumpur	2.73	101.27	0.67 ± 1.12	0.90 ± 1.86
Hanoi*	21.01	105.80	1.94 ± 2.18	0.80 ± 1.80
Watukosek	-7.46	112.43	0.71 ± 1.74	0.00 ± 2.28
Fiji	-18.13	178.40	-0.28 ± 0.84	-1.58 ± 2.46

* Hanoi dataset starts in 2004 (not 1998).

Table 6. Summary of annual tropopspheric (FT, UT and TrCO) ozone trends values for the tropics in ppbv/decade and %/decade with ±2*sigma (estimated in some cases where different units published) from TOAR-II relevant papers separated into 5 regions: Equatorial Americas, Atlantic and West Africa, East Africa, Southeast Asia and Samoa. There are 6 different references, including this work,

1089 representing ground-based and satellite observations covering the 1995-2023 time period (note that
1090 time ranges vary study to study).
1091

Region	Reference	Data Description	Time Period	FT Trends**		UT Trends**		TrCO Trends**	
				ppbv /decade[t]	% /decade	ppbv /decade[t]	% /decade	ppbv /decade[t]	% /decade
Equatorial Americas	This work	ozonesonde data from SHADOZ: San Cristobal and Paramaribo (5-10km for FT, 10-15km for UT, surface to tropopause for TrCO)	1998-2023	-0.6 ± 1.8	-0.9 ± 3.7	-2.1 ± 3.1	-3.5 ± 4.5	-0.5 ± 1.6	-1.0 ± 3.3
		IAGOS and SHADOZ data for Equatorial Americas (700-300hPa for FT)	1998-2023	0.00 ± 1.2	-0.01 ± 2.6	NA	NA	NA	NA
		OMI/MLS[$] tropospheric column (surface to tropopause)	2005-2023	NA	NA	NA	NA	1.4 ± 1.1	3.1 ± 2.5
	Gaudel et al (2024)	Fused IAGOS + SHADOZ (FT from Figure S24 and TrOC from Table 1)	2004–2019	-1.5 ± 0.75	-3.3 ± 1.7	NA	NA	-1.3 ± 0.4	-2.9 ± 0.9
	Froidevaux et al (2025)	Aura MLS UT data averaged over 147 and 215 hPa based on Figure 5 and Table S1	2005–2020	NA	NA	2.0 ± 1.3	4.0 ± 2.7	NA	NA
	Van Malderen et al (2025a)	HEGIFTOM* Paramaribo ozonesonde data (700-300 hPa for FT) from Table 2	2000-2022	0.3 ± 1.1	0.7 ± 3.0	NA	NA	NA	NA
	Boynard et al (2025)	Climate Data Record (CDR) from IASI for TrCO (surface to thermal tropopause) based on Figures 12 & 13	2008-2023	NA	NA	NA	NA	-1.8 ± 0.5	-4.0 ± 1.1
Atlantic and West Africa	This work	ozonesonde data from SHADOZ: Natal and Ascension (vertical columns same as above)	1998-2023	1.2 ± 1.8	1.9 ± 2.2	2.1 ± 2.1	3.4 ± 2.9	1.3 ± 1.1	1.9 ± 1.8
		IAGOS and SHADOZ data for Atlantic and West Africa	1998-2023	0.5 ± 1.5	0.7 ± 2.3	NA	NA	NA	NA

Region	Study	Description	Years						
		(700-300hPa for FT)							
		OMI/MLS$ tropospheric column (surface to tropopause)	2005-2023	NA	NA	NA	NA	0.7 ± 0.9	1.3 ± 1.4
	Gaudel et al (2024)	Natal/Ascension (SHADOZ only) and West Africa (IAGOS only); FT from Figure S24 and TrOC from Table 1	2004–2019	NA -0.7 ± 1.5	NA -1.3 ± 2.8	NA	NA	-0.6 ± 0.5 0.4 ± 1.0	-1.1 ± 0.9 0.7 ± 1.8
	Froidevaux et al (2025)	same as above	2005–2020	NA	NA	1.9 ± 1.3	3.7 ± 2.7	NA	NA
	Van Malderen et al (2025a;2025b)	HEGIFTOM* Ascension/Natal ozonesonde data from Table 2 (ref a) and merged Gulf of Guinea data (700-300 hPa for FT) Table S3 (ref b)	2000-2022 1995-2022	0.0 ± 1.5 -0.5 ± 0.7	0.0 ± 2.7 -1.0 ± 1.3				
	Boynard et al (2025)	CDR from IASI/Metop for TRCO (surface to thermal tropopause) based on Figures 12 & 13	2008-2023	NA	NA	NA	NA	-2.7 ± 0.5	-4.9 ± 2.0
East Africa	**This work**	ozonesonde data from SHADOZ: Nairobi (vertical columns same as above)	1998-2023	0.6 ± 1.8	0.5 ± 3.0	-1.0 ± 2.1	-1.5 ± 3.2	0.5 ± 1.3	1.1 ± 2.5
		IAGOS and SHADOZ data for East Africa (700-300hPa for FT)	1998-2023	0.5 ± 1.5	0.8 ± 2.7	NA	NA	NA	NA
		OMI/MLS$ tropospheric column (surface to tropopause)	2005-2023	NA	NA	NA	NA	0.2 ± 2.0	0.6 ± 4.5
	Gaudel et al (2024)	NA	NA	NA	NA	NA	NA	NA	NA
	Froidevaux et al (2025)	same as above	2005–2020	NA	NA	1.8 ± 1.3	3.7 ± 2.7	NA	NA
	Van Malderen et al (2025a)	HEGIFTOM* Nairobi ozonesonde data (700-300 hPa for FT) from Table 2	2000-2022	0.3 ± 1.5	0.7 ± 3.4	NA	NA	NA	NA
	Boynard et al (2025)	CDR from IASI/Metop for TRCO (surface to thermal	2008-2023	NA	NA	NA	NA	-1.8 ± 0.5	-3.6 ± 1.0

Region	Reference	Description	Period						
		tropopause) based on Figures 12 & 13							
Southeast Asia	This work	ozonesonde data from SHADOZ: Kuala Lumpur and Watukosek (vertical columns same as above)	1998-2023	0.6 ± 1.2	1.0 ± 2.5	0.0 ± 1.0	1.3 ± 3.6	1.1 ± 1.1	2.6 ± 2.3
		IAGOS and SHADOZ data for Equatorial Southeast Asia (700-300hPa for FT)	1998-2023	0.6 ± 1.3	1.6 ± 3.2	NA	NA	NA	NA
		OMI/MLS$ tropospheric column (surface to tropopause)	2005-2023	NA	NA	NA	NA	2.0 ± 2.2	5.6 ± 6.0
	Gaudel et al (2024)	Fused IAGOS + SHADOZ for SE Asia and Malaysia/Indonesia ; FT from Figure S24 and TrOC from Table 1	2004–2019	3.0 ± 1.5 1.5 ± 1.5	6.7 ± 3.3 5.0 ± 5.0	NA	NA	2.8 ± 1.4 3.4 ± 1.3	5.6 ± 2.8 8.5 ± 3.2
	Stauffer et al (2024)	ozonesonde data from SHADOZ: Kuala Lumpur and Watukosek (5-10km for FT, 10-15km for UT, surface to tropopause for TrCO)	1998-2022	0.5 ±1.0	1.3 ± 2.7	0.0 ± 1.0	1.3 ± 2.7	1.3 ± 1.0	3.4 ± 2.6
	Froidevaux et al (2025)	same as above	2005–2020	NA	NA	2.2 ± 1.6 (up to 8.0)	4.0 ± 2.8 (up to 14)	NA	NA
	Van Malderen et al (2025a;2025b)	HEGIFTOM* Kuala Lumpur alone from Table 2 (ref a) and merged SE Asia/ Malaysia data (700-300 hPa for FT) from Table S3 (ref b)	2000-2022 1995-2022	0.8 ± 1.1 3.1 ± 1.1	2.2 ± 3.0 6.2 ± 2.2	NA	NA	NA	NA
	Boynard et al (2025)	CDR from IASI/Metop for TRCO (surface to thermal tropopause) based on Figures 12 &13	2008-2023	NA	NA	NA	NA	0.0 ± 0.5	0.0 ± 1.4
Samoa	This work	ozonesonde data from SHADOZ: Samoa (vertical columns same as above)	1998-2023	0.6 ± 1.8	0.8 ± 4.4	0.0 ± 4.1	-1.3 ± 9.2	-0.5 ± 1.8	-1.4±4.8

	IAGOS and SHADOZ data for Samoa (700-300hPa for FT)	1998-2023	-0.15 ± 1.5	-0.4 ± 3.8	NA	NA	NA	NA
	OMI/MLS[$] tropospheric column (surface to tropopause)	2005-2023	NA	NA	NA	NA	2.5 ± 2.3	9.1 ± 8.3
Gaudel et al (2024)	Samoa (SHADOZ only) ;TrOC from Table 1	2004–2019	NA	NA	NA	NA	-1.1 ± 1.9	-3.1 ± 5.4
Froidevaux et al (2025)	same as above	2005–2020	NA	NA	1.9 ± 1.5	3.4 ± 2.6	NA	NA
Van Malderen et al (2025a)	HEGIFTOM* Samoa ozonesonde data (700-300 hPa for FT) from Table 2	2000-2022	-0.07 ± 1.3	-0.2 ± 4.2	NA	NA	NA	NA
Boynard et al (2025)	CDR from IASI/Metop for TRCO (surface to thermal tropopause) based on Figures 12 & 13	2008-2023	NA	NA	NA	NA	-2.7 ± 0.5	-9.0 ± 1.7

* Note HEGIFTOM data include measurements from the following ground networks: IAGOS, ozonesondes, FTIR, Dobson Umkehr, and Lidar.

** Annual average trend plus 2*sigma.

[t] SHADOZ Trends have been converted from DU/decade to ppbv/decade for each layer so these are approximate values based on Tables 1 and 2.

[$] OMI/MLS trend values are from the 5x5 deg box that contains the SHADOZ station. In the cases where there are two SHADOZ stations (Nat/Asc, KL/Java, SC/Para), the trend is the average of the two individual OMI/MLS trends and confidence interval values.

1106
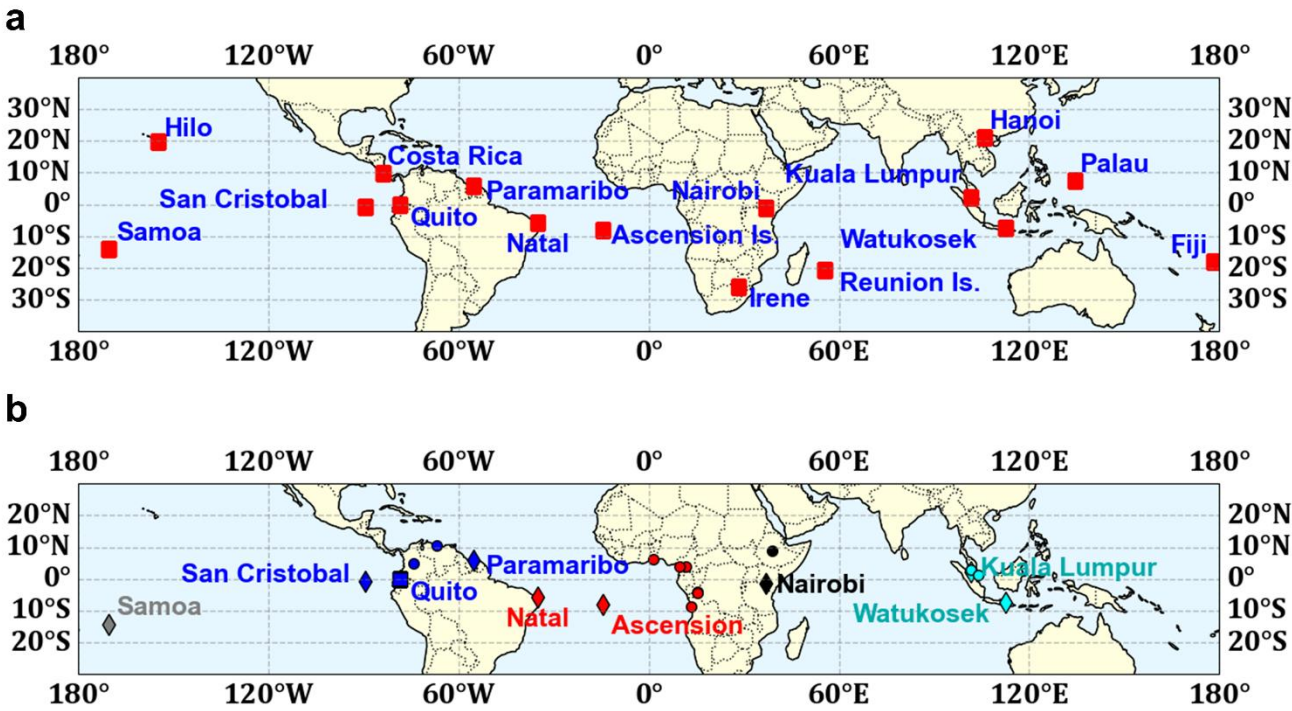
1107
1108
1109 **Figure 1.** (a) Map of all SHADOZ stations in 2025 when the Quito and Palau records, that began in 2014
1110 and 2016, respectively, joined the network. (b) SHADOZ sites used in T21 for 1998-2019 equatorial
1111 trends and here for 1998-2023 trends are represented with diamonds. SHADOZ stations whose
1112 combined records are examined within regions are colored blue for Equatorial Americas, red for
1113 Atlantic and cyan for equatorial southeast Asia. The airport locations from IAGOS include those
1114 indicated with circles: red for Atlantic and West Africa, black for East Africa, cyan for the equatorial
1115 Southeast Asia region. For T21 and the trends here, the fifth station, including the combined stations, is
1116 Samoa (in gray). Quito (blue square) data are included in the Equatorial Americas trends of **Table 3**. All
1117 station and airport locations are in **Table 1.** The 5 SHADOZ sites (2 individual and 3 combined) from
1118 T21 and for which trends are updated here appear in **Table 2** with the MLR trends. Individual SHADOZ
1119 and IAGOS site names within each region and their trends are shown in **Table 3**. Trends computed by
1120 QR for total column and FT ozone at 13 individual SHADOZ stations are summarized in **Table 4**.
1121
1122
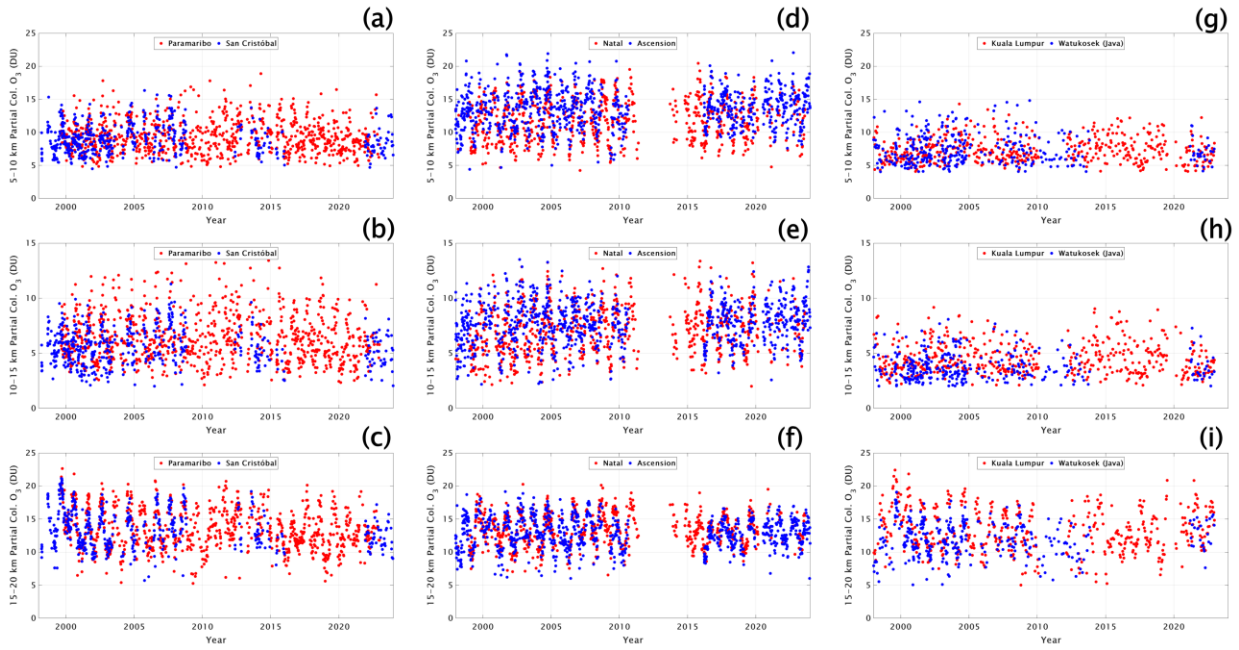
1123
1124
1125 **Figure 2.** Time-series of ozone column segments (in DU) for the combined SHADOZ stations, for the
1126 layers 5-10 km, 10-15 km, 15-20 km for: San Cristóbal-Paramaribo (a-c); Natal-Ascension (d-f); Kuala
1127 Lumpur-Watukosek (Java) (g-i). Station coordinates in **Table 1.**
1128
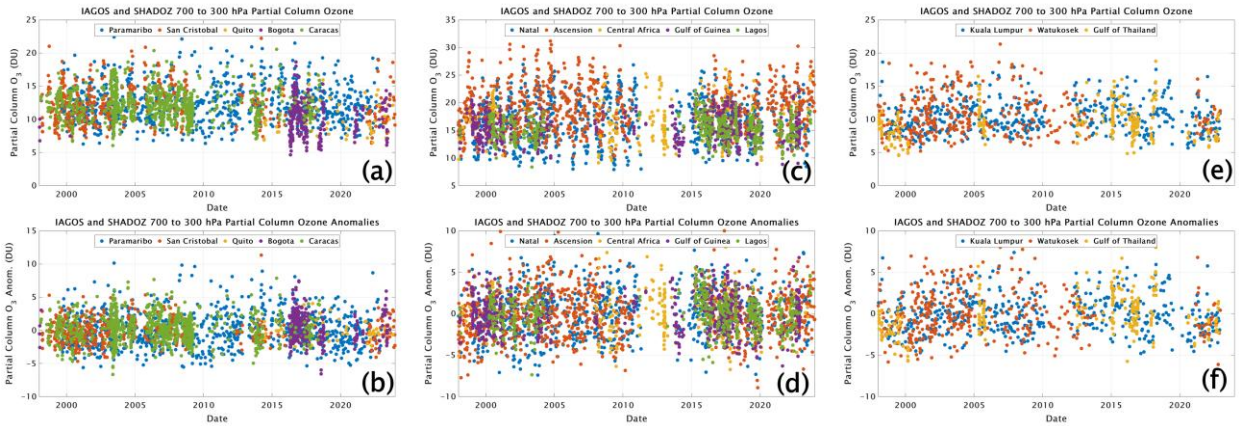
1129
1130
1131 **Figure 3.** Time-series of SHADOZ and IAGOS partial ozone column amounts and partial ozone column
1132 anomalies (in DU) for the pressure-defined mid-free troposphere, FTp (700 to 300 hPa), for (a-b)
1133 Equatorial Americas, (c-d) Atlantic and West Africa, and (e-f) Equatorial SE Asia. The listing of the
1134 individual sites included in these datasets appears in **Table 3**. Coordinates are in **Table 1.**
1135
1136
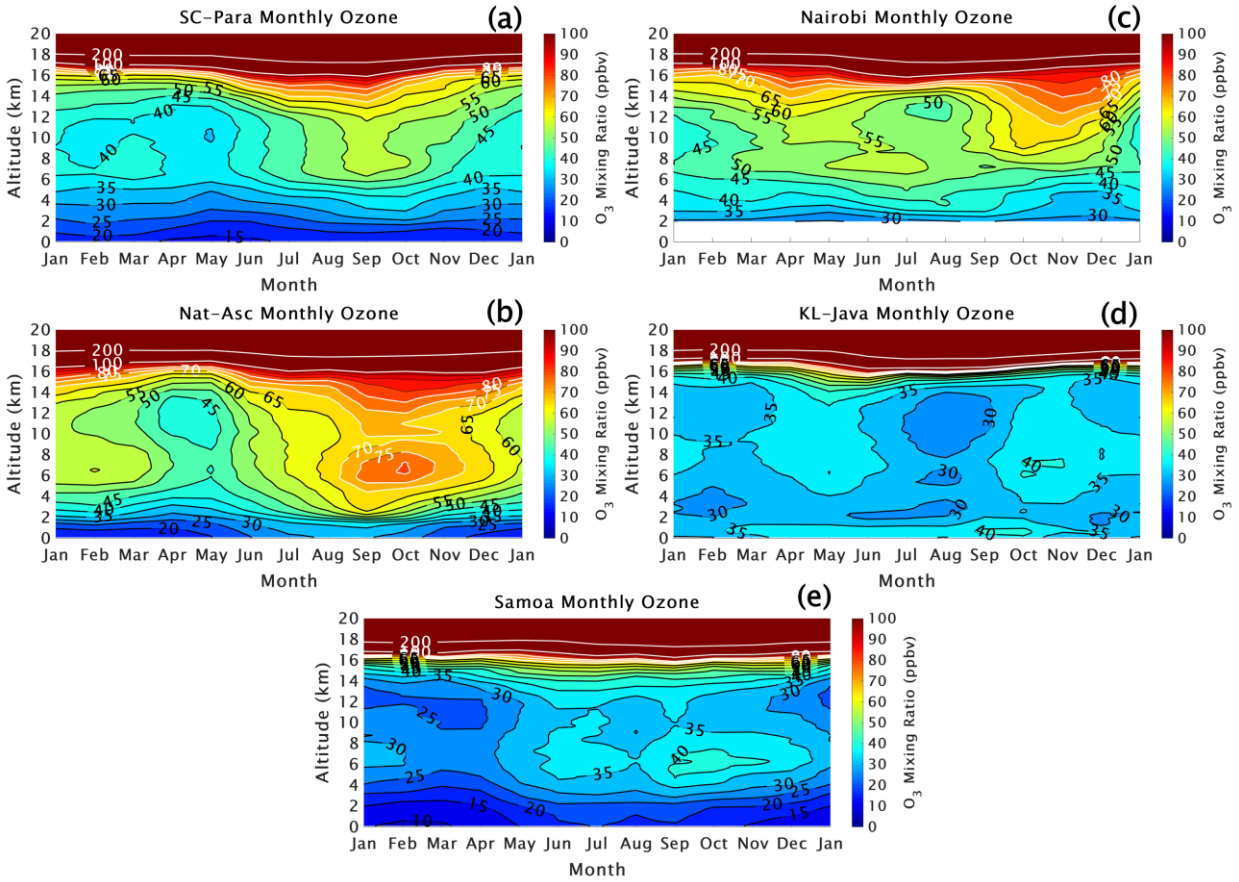
1137
1138 **Figure 4.** Monthly averaged ozone mixing ratios from the surface to 20 km altitude for the five SHADOZ sites: (a)
1139 San Cristóbal – Paramaribo, (b) Natal – Ascension Island, (c) Nairobi, (d) Kuala Lumpur – Watukosek (Java), and
1140 (e) Samoa. Colors with black and white contour lines are shown for the ozone mixing ratios in ppbv.
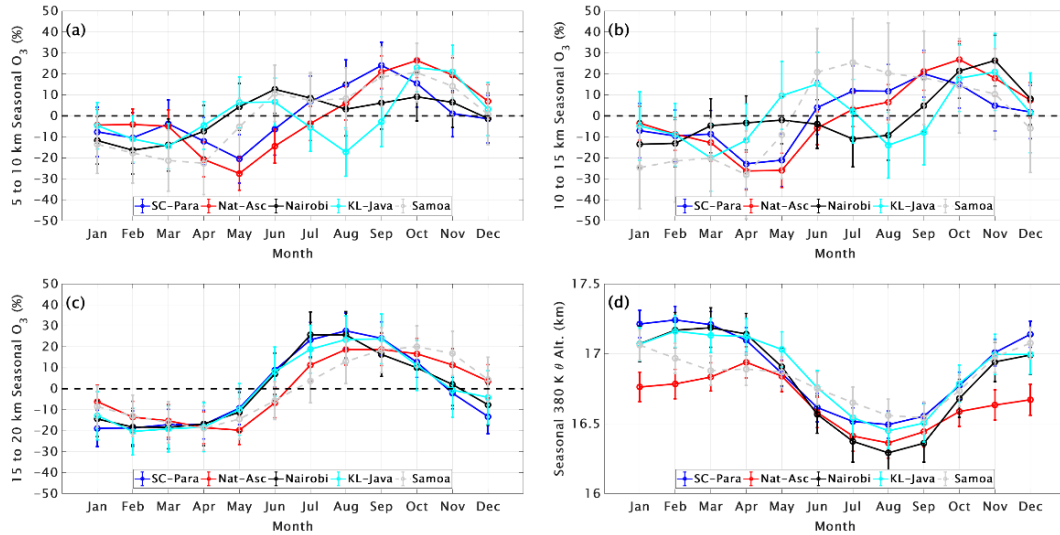
1141
1142 **Figure 5**. Monthly ozone variability for the five T21 SHADOZ profiles, expressed as percent anomaly from annual
1143 mean, determined from the MLR model in the lower and middle FT (5-10 km: a, 10-15 km: b) and for the LMS (15-
1144 20 km: c). The tropopause Height (TH) seasonal cycle (d, in km) is based on the 380 K potential temperature
1145 surface from the radiosondes. Dots indicate monthly values; error bars display the 95% confidence intervals.
1146
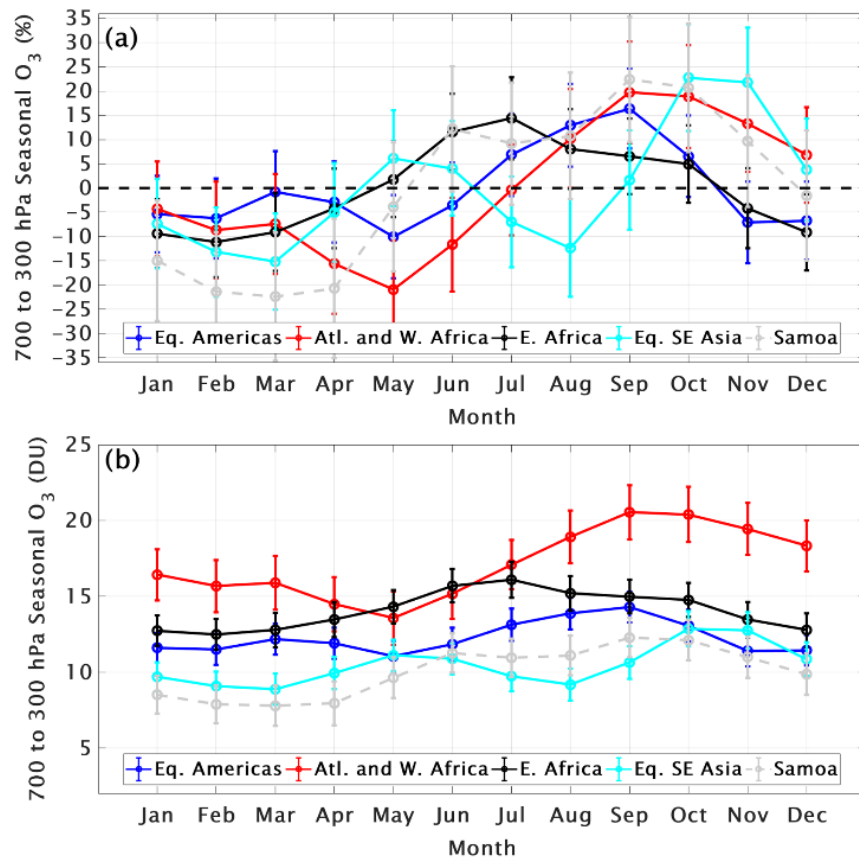
1147
1148
Figure 6. Monthly ozone variability for the five combined SHADOZ+IAGOS regions (defined in **Figure 1** and **Table 3**), expressed as anomaly from annual mean in (a) percent with actual values in DU (b), for the FTp (700-300 hPa) column. Dots indicate the monthly values; error bars display the 95% confidence intervals.

1153
1154
1155
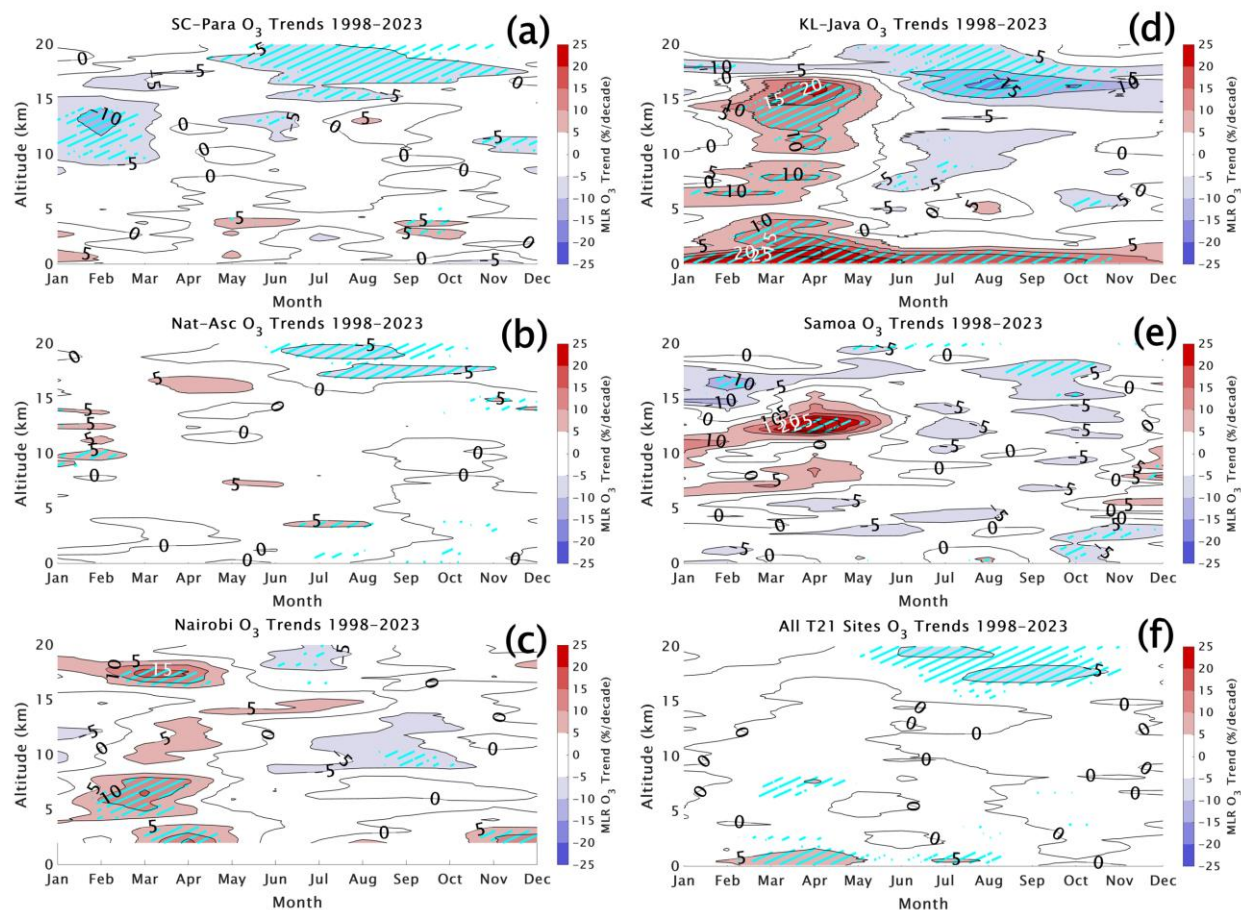
Figure 7. Monthly MLR ozone linear trends from 0 to 20 km in percent per decade for the SHADOZ T21 stations (a) San Cristóbal-Paramaribo (SC-Para); (b) Natal-Ascension (Nat-Asc) (c) Nairobi, (d) Kuala Lumpur-Watukosek (KL-Java); (e) Samoa. This is an update to Figure 6 in T21. In (f), average trends over (a) through (e) are displayed by combining the records from all eight individual T21 SHADOZ stations. Positive trends are shown in red shades and negative trends are shown in blue shades. Trends with p-values <0.05 (exceeding the 95% confidence interval) are shown with cyan hatching.
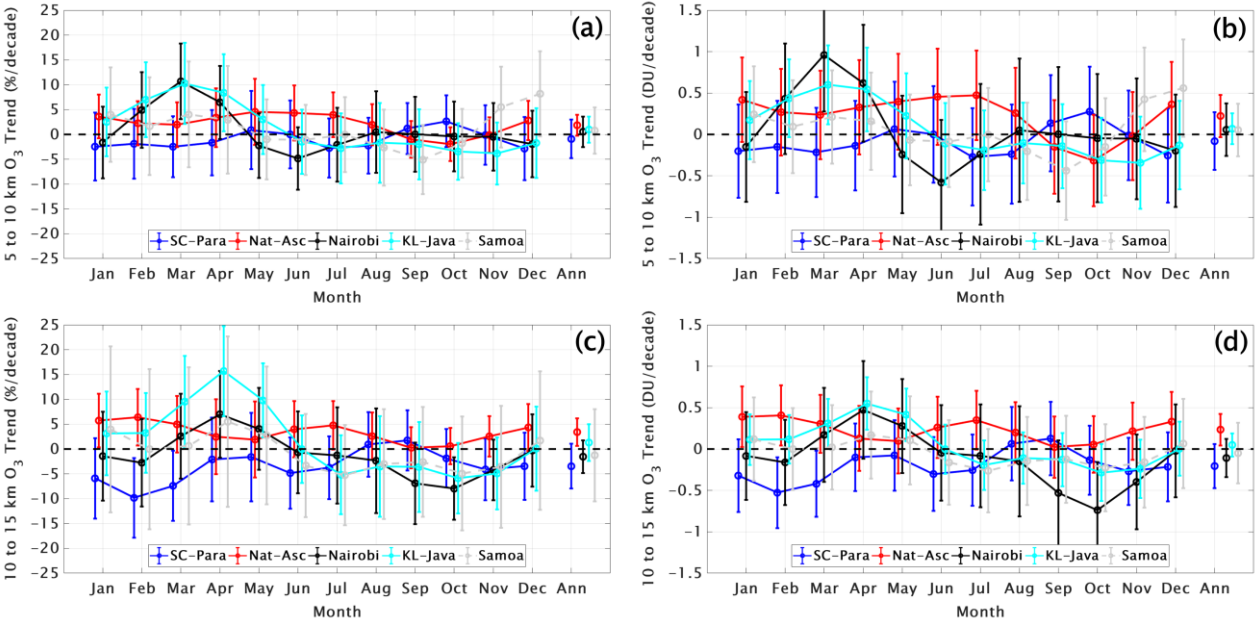
Figure 8. Monthly and annual MLR trends for five T21 SHADOZ sites in lower FT ozone column, integrated from 5-10 km, for (a) %/decade (b) DU/decade; (c) and (d) same as (a) and (b) respectively but for upper FT ozone column (10-15 km), derived from SHADOZ sondes. Dots indicate the monthly and annual (at right in each frame) trends; error bars display the 95% confidence intervals.
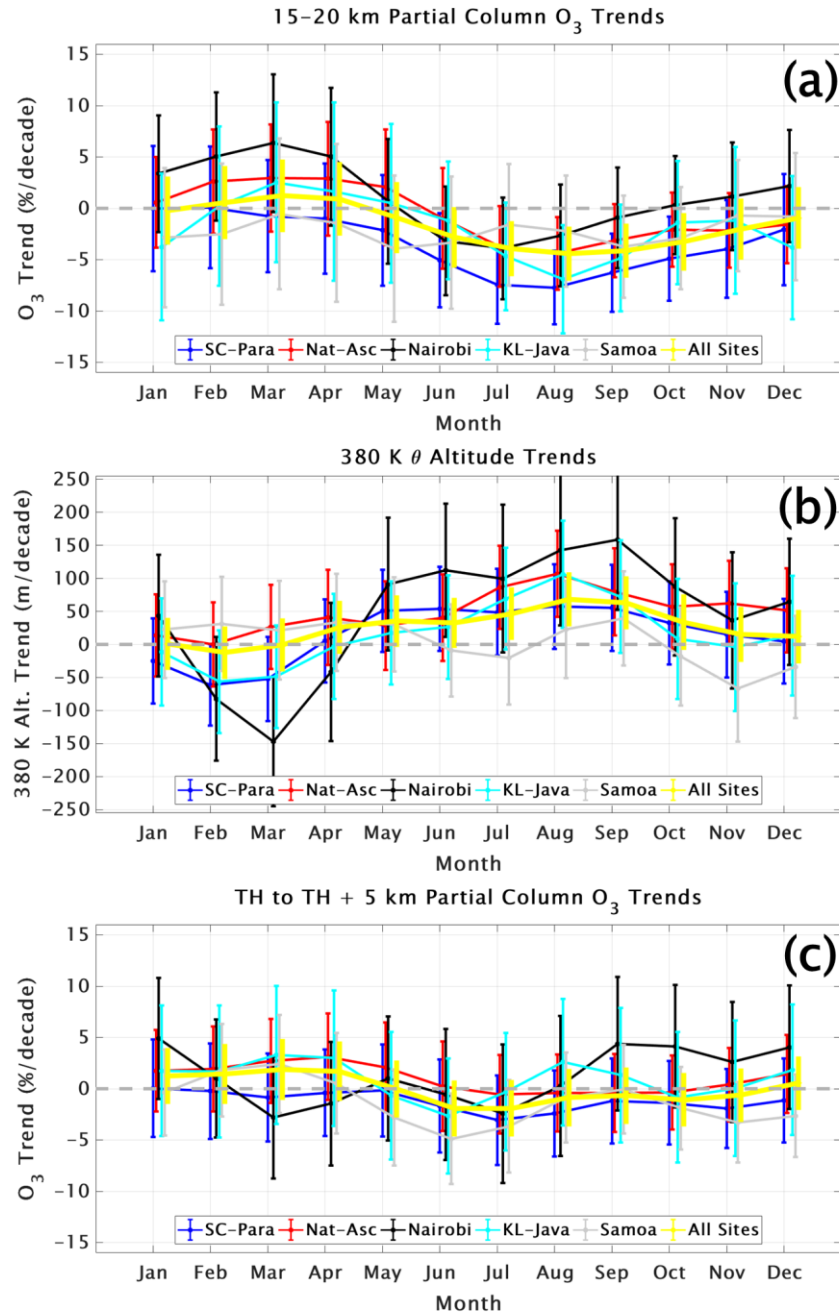
1174
Figure 9. (a) Monthly MLR trends (colored dots) derived from SHADOZ T21 stations
highlighting a July-October decrease in LMS ozone in 15-20km layer; yellow dots denote the
mean of all T21 stations, with error bars indicating the 95% confidence intervals. (b)
Corresponding TH trends (380 K potential temperature; θ) derived from the radiosondes. (c)
Same as (a) except trends have been computed for the segments between the tropopause and 5
km above the TH. Compared to (a) the trends in the tropopause referenced ozone column (c)
become close to zero throughout the year.

1182
1183
1184
1185
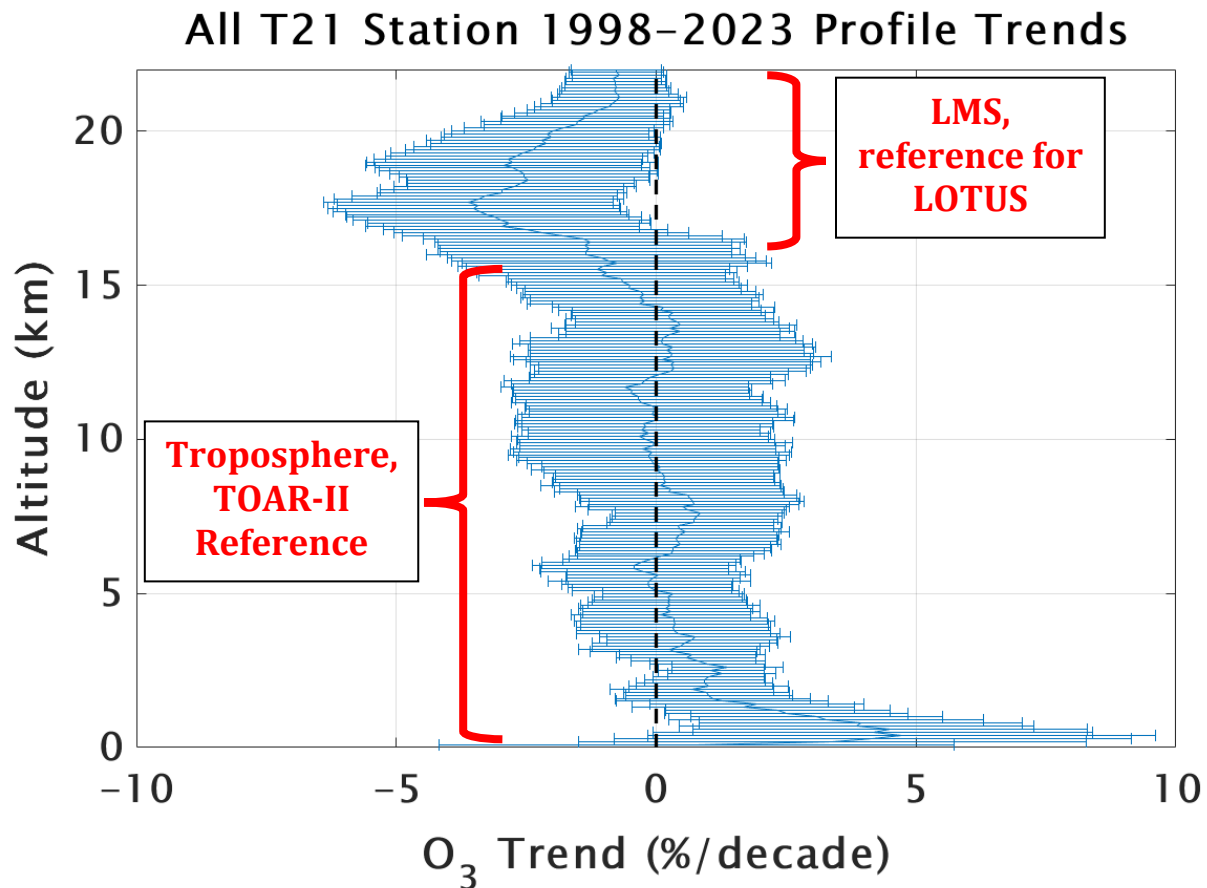
Figure 10. The total mean annual ozone trend (solid blue line), based on mixing ratio changes in 100-m intervals, from the surface to 22 km for all eight T21 SHADOZ profile datasets in %/decade with the 95% confidence interval range denoted. The LMS region is of interest to the stratospheric community, e.g., the LOTUS activity, whereas the tropospheric segment is marked as the primary TOAR-II focus. The -4%/decade trend in LMS ozone is similar to that derived from satellites in that region. The mean change throughout the FT is negligible and within the uncertainty range except below 2 km where mean increases ~+5%/decade are indicated. The near-surface trends are primarily a result of rapid increases in urbanized regions of equatorial SE Asia (Stauffer et al., 2024).

1196   (a)

1197   **(b)**

1198
1199

1200 **(c)**

1201
1202 **(d)**
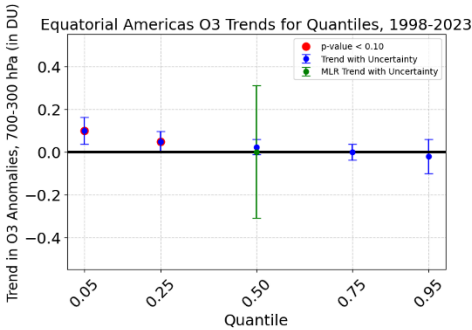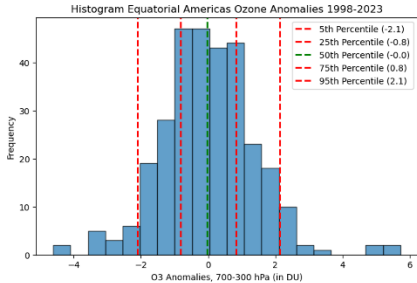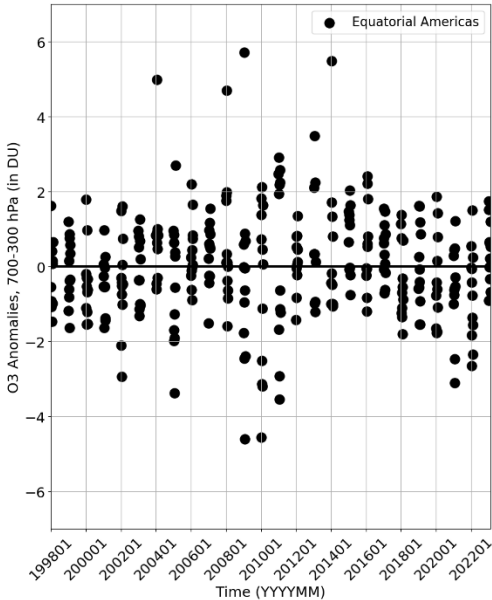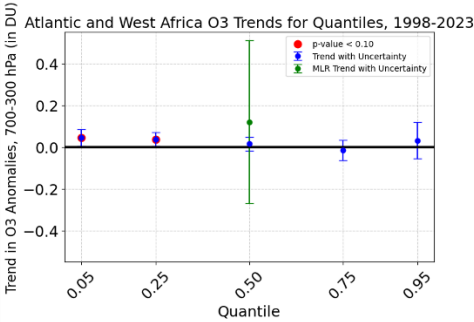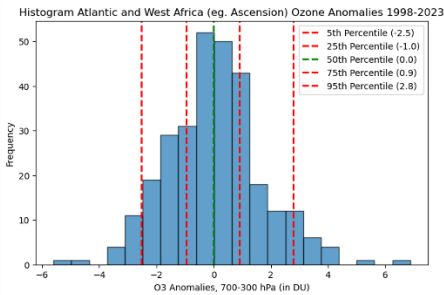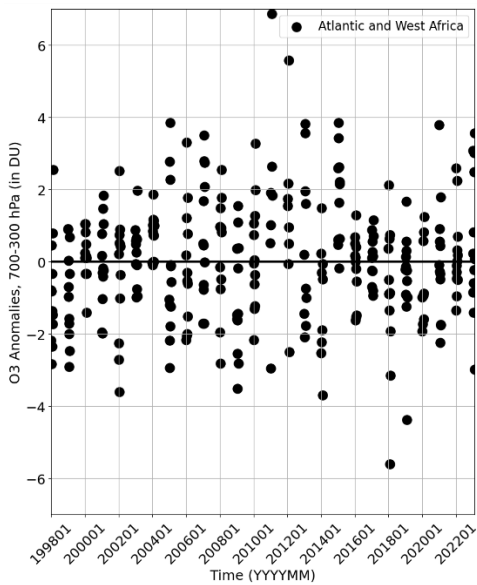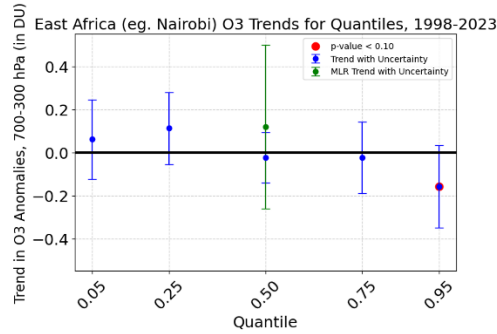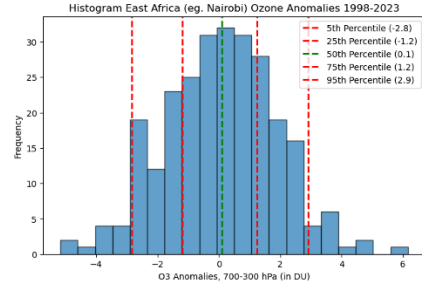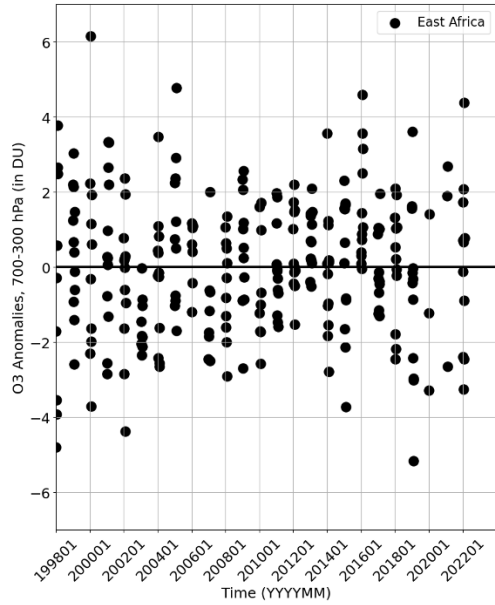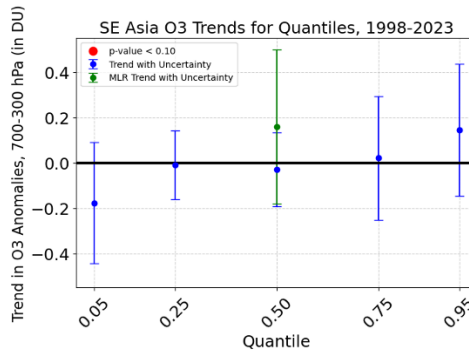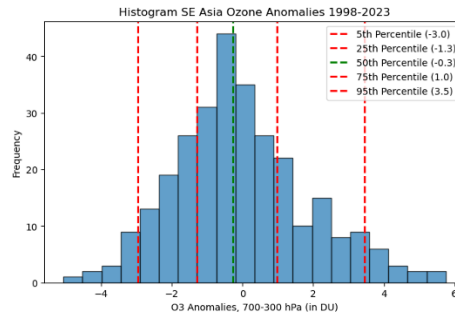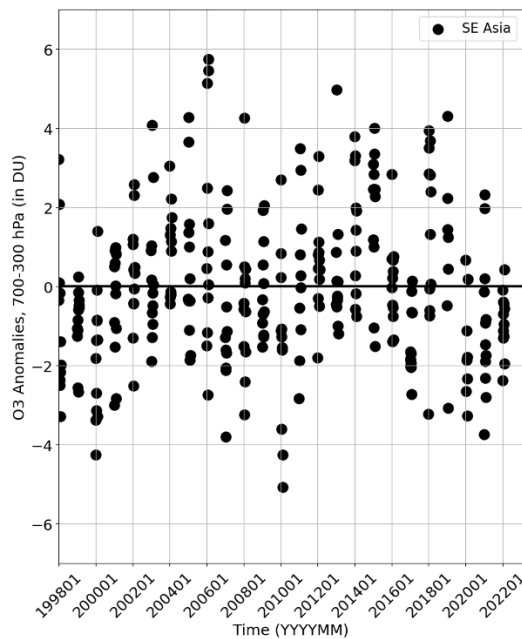
1203
1204
1205
1206 **Figure 11.** FTp column ozone segment anomalies (monthly means) from SHADOZ sondes and IAGOS data, as
1207 described in **Table 3.** Each frame displays the anomalies timeseries in DU at the left, a histogram of those
1208 anomalies in DU (each has a unique scale, ozone anomaly values for each percentile (dashed lines) are in
1209 parentheses) and the trends distribution by quantiles. Trends from annual MLR ozone (median, 50%-ile) over
1210 1998-2023 are green circles with their respective +/- 2sigma bars. The same period trends computed with QR by
1211 quantiles (0.05= lowest 5%-ile), 0.25 (25%-ile), 0.50 for median trends, 0.75 (75%-ile) and 0.95 (95%-ile) are blue
1212 circles. Red circles denote p<0.10. (a) equatorial Americas; (b) Atlantic and West Africa region; (c) east Africa; (d)
1213 equatorial southeast Asia.
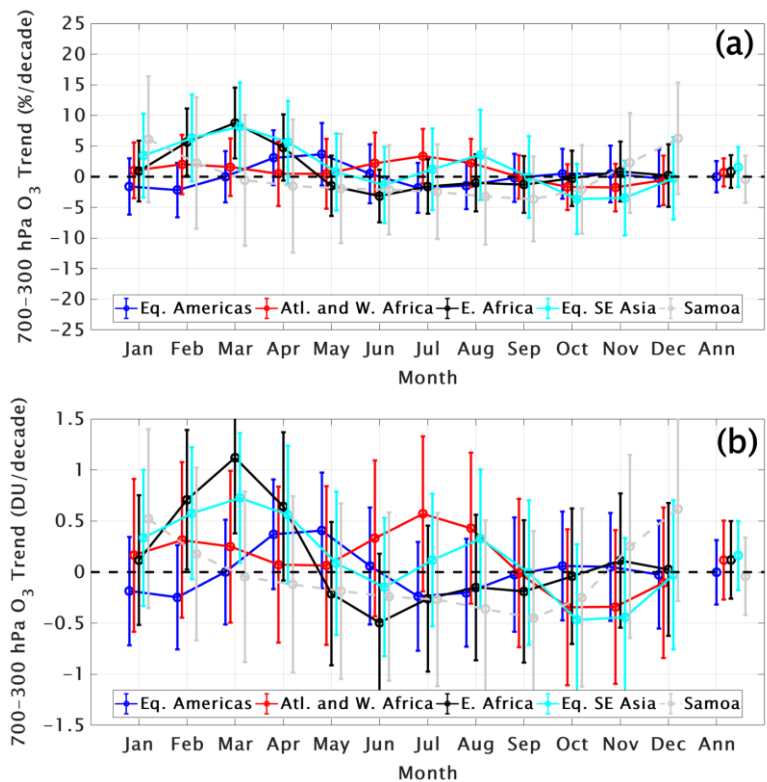
1216 **Figure 12.** Monthly and annual MLR ozone trends for 5 combined SHADOZ+IAGOS regions, defined in **Table 3**, for
1217 FTp column in (a) %/decade and (b) DU/decade. Dots indicate the monthly and annual trends, whereas error bars
1218 display the 95% confidence intervals.
1219
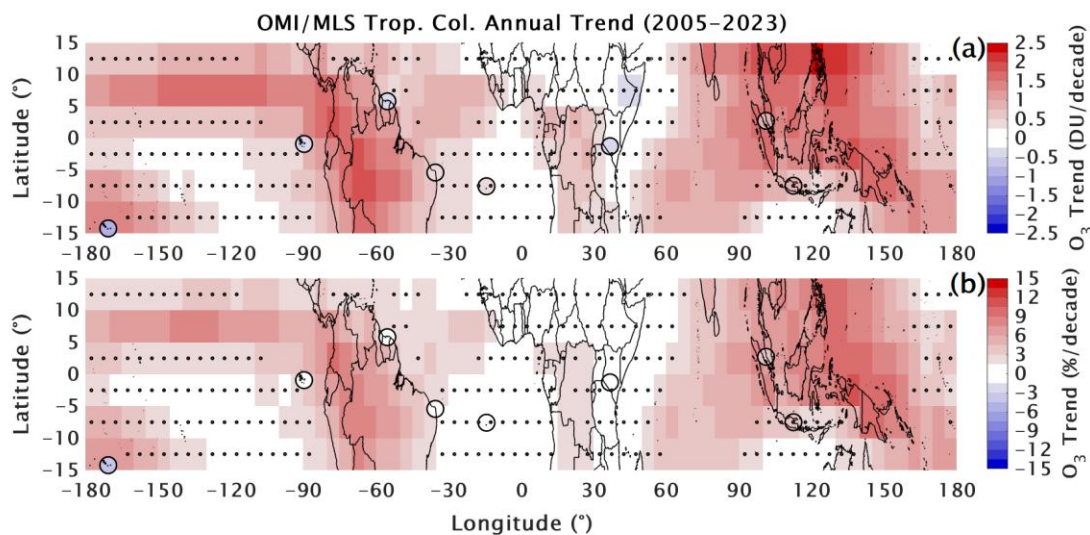
1220
1221 **Figure 13.** The most recent trends, 2005-2023, shown for the equatorial region based on updated
1222 OMI/MLS tropospheric total column ozone (TrCO$_{satellite}$) estimates in which a ~1% per decade positive
1223 drift in OMI was corrected. (a) in DU/decade; (b) in %/decade. The corresponding SHADOZ-derived
1224 TrCO$_{sonde}$ column changes for 2005-2023 are superimposed on the map. Stippling indicates where
1225 OMI/MLS trends *do not* exceed the 95% confidence interval (i.e., historically referred to as statistically
1226 insignificant).
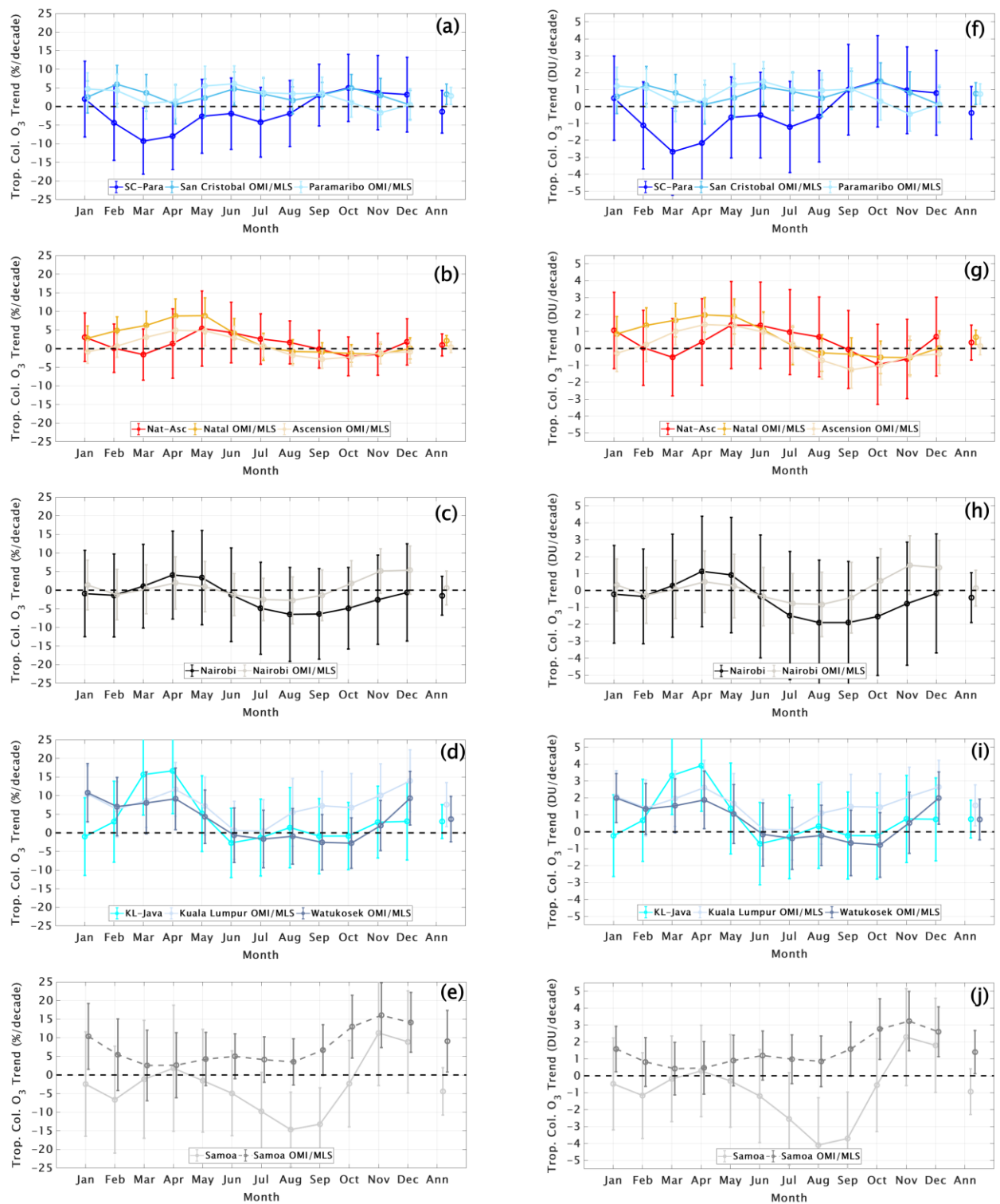
1227
1228 **Figure 14.** Monthly and annual MLR ozone trends in total tropospheric column (defined using
1229 the WMO lapse rate tropopause; TrTO) for the five T21 stations and the OMI/MLS pixel for each
1230 individual SHADOZ station each region. Dots indicate the ozone trend in % (a-e) and DU (f-j)
1231 per decade; error bars show the 95% confidence intervals.
1232
1233 *Supplement to:*
1234

Tropical Tropospheric Ozone Trends (1998 to 2023): New Perspectives from SHADOZ, IAGOS and OMI/MLS Observations

Anne M. Thompson et al. (Correspondence to: anne.m.thompson@nasa.gov)
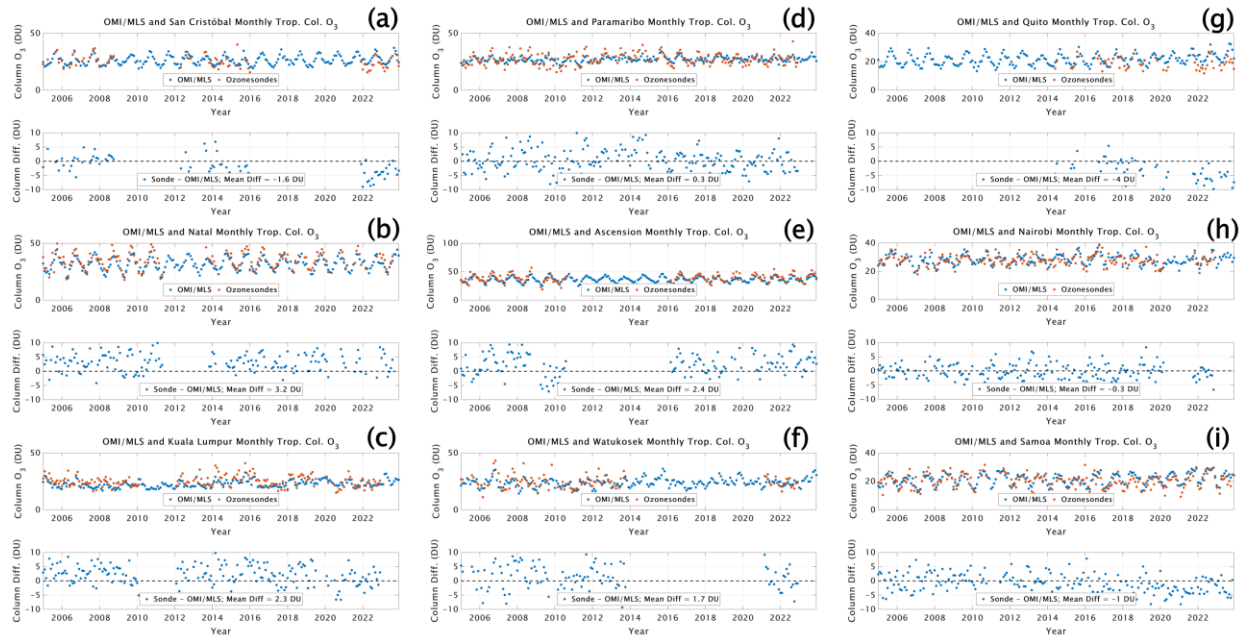
Supplementary Figure S1. For the nine SHADOZ stations analyzed (eight T21 plus Quito), the upper panels in (a) –(i) give monthly mean tropospheric column ozone, $TrCO_{sonde}$, in DU, estimated from the most recent OMI/MLS residual satellite product (Gaudel et al., 2024) and integrated from surface to tropopause from SHADOZ data. Tropopauses for both the integrated ozonesonde column and the OMI/MLS column estimate are determined using the WMO lapse rate tropopause. In text, the column integrals are referred to as $TrCO_{saellite}$ for the OMI/MLS and $TrCO_{sonde}$ for the SHADOZ data. Lower panels give the difference between the two tropospheric columns in DU (blue) with the mean difference over the periods of record indicated in the legend (ozonesonde-OMI/MLS).